Spring 5-7-2021

Active Blade Pitch and Hull-Based Structural Control of Floating Offshore Wind Turbines

Eben Lenfest
University of Maine, eben.lenfest@maine.edu

ACTIVE BLADE PITCH AND HULL-BASED STRUCTURAL CONTROL OF FLOATING OFFSHORE WIND TURBINES

By

Eben J. Lenfest

B.S., University of Maine, 2019

A THESIS

Submitted in Partial Fulfillment of the

Requirements for the Degree of

Master of Science

(in Mechanical Engineering)

The Graduate School

The University of Maine

May 2021

Advisory Committee:

Dr. Andrew Goupee, Associate Professor of Mechanical Engineering, Advisor

Dr. Richard Kimball, Presidential Professor in Ocean Engineering and Energy

Dr. Babak Hejrati, Assistant Professor of Mechanical Engineering

ACTIVE BLADE PITCH AND HULL-BASED STRUCTURAL CONTROL OF FLOATING OFFSHORE WIND TURBINES

By Eben J. Lenfest

Thesis Advisor: Andrew Goupee

An Abstract of the Thesis Presented
in Partial Fulfillment of the Requirements for the
Degree of Master of Science
(in Mechanical Engineering)
May 2021

Floating offshore wind turbines have the potential to bring renewable energy to waters too deep for traditional offshore wind turbines while still being able to harness strong coastal winds in areas near population centers. However, these floating wind turbines come at a higher capital cost relative to fixed foundations and are more susceptible to vibrations induced by waves. Advances in control technologies offer the potential to reduce fatigue loads due to these vibrations, extending the life of the platform and thereby spreading the capital costs of the turbine over a longer period of time. One such advance is in blade pitch control, a standard component of most modern wind turbines. Existing solutions for adapting the blade pitch controller for use on a floating platform either detune the controller with the result of slowed response, make use of complicated tuning methods, or incorporate a nacelle velocity feedback gain. With the goal of developing a simple control tuning method for the general FOWT researcher that is easily extensible to a wide array of turbine and hull configurations, this last idea is built upon by proposing a simple tuning strategy for the feedback gain. This strategy uses a two degree-of-freedom (DoF) turbine model that considers tower-top fore-aft and rotor angular displacements. For evaluation, the nacelle velocity term is added to an existing gain scheduled proportional-integral controller as a proportional gain. The modified controller is then compared to baseline

land-based and detuned controllers on semisubmersible, spar, and TLP systems for several load cases. Results show that the new tuning method balances power production and fatigue load management effectively, demonstrating that it is adaptable to many different types of hulls. This makes it useful for prototype design. Advances in hull-based structural control are also considered through the evaluation and development of a gain schedule for a novel type of adjustable tuned mass damper known as a ducted fluid absorber. This type of tuned mass damper uses compressed air to adjust its natural frequency, and so the amount of power consumed by the compressors is evaluated relative to the output of the wind turbine. Performance of a hull designed for ducted fluid absorbers is evaluated for several incoming wave directions to ensure consistent performance, and the potential for extracting electricity from the ducted fluid absorbers is considered. Finding the dampers to be feasible for use, a method of scheduling the settings of these dampers to minimize the standard deviation of a platform rigid-body mode of choice is developed. The addition of the dampers is found to produce significant reductions in the magnitude of several vibration modes, though the advantages of actively controlling the damper setting are small relative to those of simply having the dampers.

DEDICATION

This work is dedicated to Mom, Dad, Luke, and Raina, for their ceaseless inspiration and support.

ACKNOWLEDGEMENTS

I would like to gratefully acknowledge the support of the National Science Foundation through Award Number 1832876, as well as support given by AVANGRID in the form of a master's fellowship.

I'm grateful to Alan Wright, Nikhar Abbas and Andrew Goupee for their contributions on the topic of generic blade pitch controllers. Additional thanks go to Daniel Zalkind, Matt Shields, Christopher Allen, and Andrew Goupee for their contributions on the topic of hull-based ducted fluid absorbers.

TABLE OF CONTENTS

LIST OF TABLES

LIST OF FIGURES

LIST OF NOMENCLATURE

$\overline{C}_{FOWT}$	FOWT pitch damping (radiation plus linearized viscous
c	Linear damping from a single TMD
h_{hub}	Hub height
H_s	Significant wave height
$H(\omega)$	Hull RAO
I_{drive}	Combined rotor and drivetrain rotational inertia
$\overline{I}_{FOWT}$	FOWT pitch inertia (physical and added)
$\overline{K}_{FOWT}$	FOWT pitch stiffness (hydrostatic plus mooring)
k_i	Integral gain on rotor speed error
k_p	Proportional gain on rotor speed error
k_{px}	Proportional gain on tower-top velocity
L_{hh}	Hub height as measured from platform pitch axis
M_y	Tower-base pitching moment
P	Generator power
P_{damp}	Power dissipated by TMDs
p	damper pressure
Q_{aero}	Aerodynamic torque
$Q_{gen,lss}$	Generator torque cast at the low-speed shaft
s_i	i^{th} system pole
$S(\omega)$	Wave power spectrum
T_{aero}	Aerodynamic thrust
T_p	Peak wave period
V	Damper volume
v	Wind velocity
v_{damp}	TMD velocity

W	Expansion work
x	Tower-top fore-aft displacement
β	Blade pitch angle
γ	JONSWAP peak enhancement factor
$\Delta\zeta_{DoF}$	Additional tower-top feedback FOWT damping on specified DoF
$\zeta_{rot,des}$	Controller design damping ratio
θ	FOWT pitch angle
σ	Standard deviation
ϕ	Rotor angular displacement
ω	Forcing frequency
$\omega_{n,rot,des}$	Controller design frequency
Ω	Rotor angular velocity

LIST OF ACRONYMS AND ABBREVIATIONS

DFA	Ducted Fluid Absorber
DLC	Design Load Case
DoF	Degree of Freedom
FOWT	Floating Offshore Wind Turbine
JONSWAP	Joint North Sea Wave Observation Project
NREL	National Renewable Energy Laboratory
ROSCO	NREL's Reference OpenSource Controller
TLP	Tension Leg Platform

CHAPTER 1

INTRODUCTION

1.1 Motivation

As the effects of climate change are beginning to be felt, the drive to make green energy sources more affordable and competitive with existing energy technologies has been increasing. Wind power is one of the more prevalent forms of green energy, and a recent focus of research in this area has been on the development of floating offshore wind platforms. Some of the advantages of this type of wind power are seen in Figure 1.1, reproduced from [1]. Many of the areas of high average wind speed in the U.S., denoted in dark blue, are found in coastal waters. Additionally, these sites are close to major population centers, leading to less transmission loss.

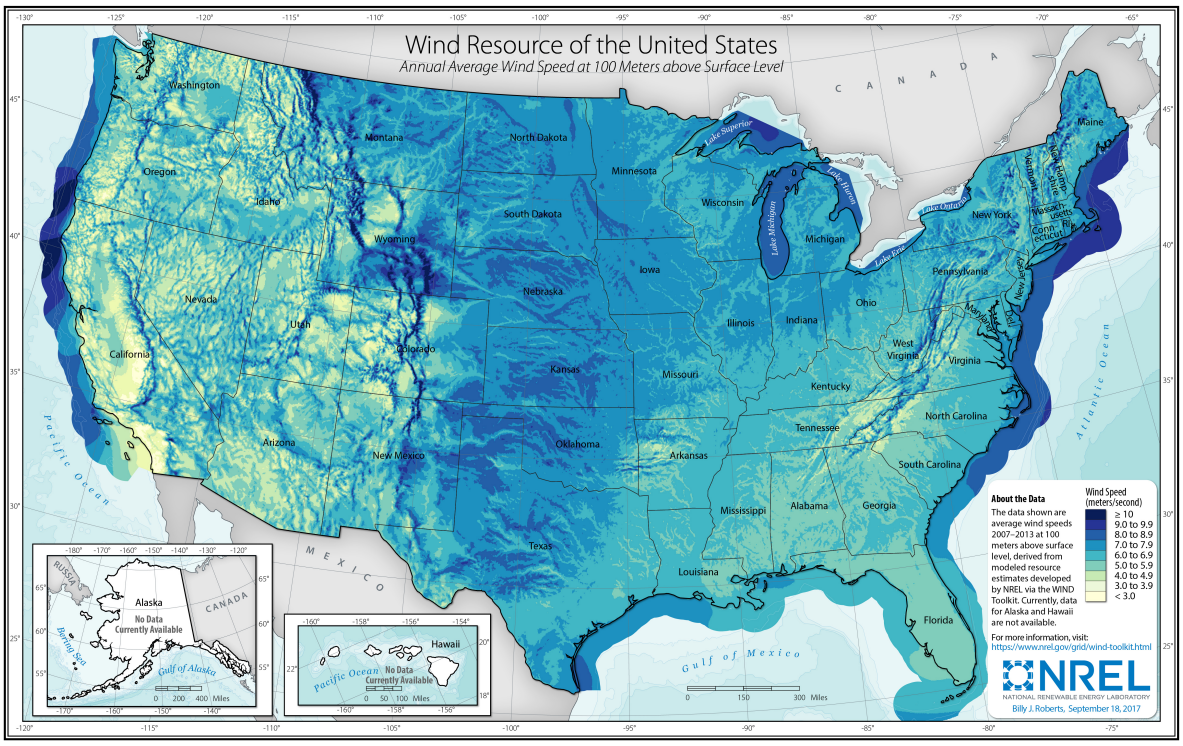

Figure 1.1. Wind resource of the United States at 100m, reproduced from [1]

While fixed-bottom offshore wind turbines also share these advantages, they are limited to shallow areas (typically less than 60m). As can be seen in Figure 1.2, reproduced from [2], much of the seaboards of the U.S. are in greater depths than this. This necessitates the use of floating foundations.

Figure 1.2. Water depths for the coasts and Great Lakes of the United States of America, reproduced from [2]

The issue with floating foundations is that they result in greater structural vibration due to wind and wave loading, as well as inertial loading due to the rigid-body motion. This causes structural fatigue that could reduce the useful life of the platform, and it also affects the amount and consistency of the power produced by the generator. There are several avenues for tackling this problem, including modifications to the wind turbine's active blade pitch controller and the addition of hull-mounted tuned mass dampers (TMDs).

1.2 Background

1.2.1 Blade Pitch Controllers for Floating Wind Turbines

The challenge with adapting the blade pitch controller to control platform motion is that it is already tasked with regulating power production. This is complicated further due to an effect known as the negative damping problem [3, 4]. When a turbine is mounted on a floating platform, the nacelle translates forward and backward relative to the wind. As the nacelle moves forward, its velocity relative to the wind increases. This causes the pitch controller to feather the blades slightly to reduce generator speed. The thrust force on the turbine is thereby reduced, further accelerating the nacelle forward. The inverse effect is seen as the nacelle moves backward. The rigid-body pitch (or in the case of tension leg platforms, surge) natural frequency of the platform can be excited through these oscillations, reducing the stability of the system.

There are several proposed solutions for tackling this issue. The most basic of these, proposed by Larsen and Hanson [2], is to detune the gains of the blade pitch controller until it can no longer respond fast enough to excite the platform motion. While platform pitching is reduced using this control scheme, it can lead to poor power regulation.

Feedforward control has also been used to address the issue; LiDAR can be used to detect incoming wind and set blade pitch accordingly [5]. Investigations into the implementation of LiDAR have mostly returned positive results. Studies by Schlipf et al. [6, 7] and Navalkar et al. [8] all found that predictive control reduces power and generator speed variations while simultaneously decreasing loads on the tower, shaft, and blades.

Many other approaches to floating wind turbine control have been explored, of varying degrees of complexity. Magar and Balas [9] implemented an adaptive, individual blade-pitch controller that feeds back platform pitch, and found that it outperformed baseline controllers but could not guarantee stability. Lemmer et al. [10] consider the benefits of supplanting traditional proportional-integral (PI) controllers with an optimized Linear Quadratic Regulator (LQR). The LQR is found to be superior at managing

platform motions and resonance. In another study, an adaptive state feedback controller was designed to accommodate change in the first tower natural frequency due to aging [11]. Fatigue loads on the support structure were reduced by 3%. The work of Kakita et al. [12] involved finding the optimum gains for a traditional PI controller using the Fictitious Reference Iterative Tuning (FRIT) approach. Generator speed and platform pitching were improved over the baseline, but blade pitch actuation increased significantly.

One other option for eliminating the instability is to estimate the absolute wind speed by providing feedback to the controller in the form of the nacelle velocity or acceleration. This was explored by Fischer [13], who found reduced platform pitching and rotor overspeed but increased drivetrain loads. Fischer and Loepelmann [14] later found that by feeding back a reduced frequency range to the generator torque controller, these loads could be decreased. Another study [15] found similar improvements in tower bending loads. Lackner [16] made the rotor speed setting a variable of nacelle velocity, resulting in better platform stability but more rotor speed variation. A controller developed by Skaare et al. [17] focused on extending platform fatigue life, and did so by at least 86% at the expense of a 3.8% reduction in power output relative to a conventional controller.

While there are a wealth of options for blade pitch controller tuning, the gap that this work hopes to address is to produce a simple method for generating controller gains that will provide adequate performance in both power and pitch regulation for researchers who don't necessarily specialize in controls. Something like this might therefore be useful to integrate into a controller design tool like ROSCO [18]. This tuning approach will utilize feedback of nacelle velocity, as it is relatively easy to implement, does not require feedforward control hardware, and has seen promising results in past research.

An overview of wind turbine operating regions is given in Figure 1.3. The controller presented here is focused on region 3, which spans from the wind turbine's rated wind speed to cut-out wind speed. Power production starts at cut-in, the border between region 1 and region 2. From there up to the rated wind speed, the power produced by the turbine

is maximized using torque control of the turbine. In region 3, beyond the rated wind speed, active blade pitch control is used to regulate power in winds sufficiently high to produce the nameplate capacity of the wind turbine.

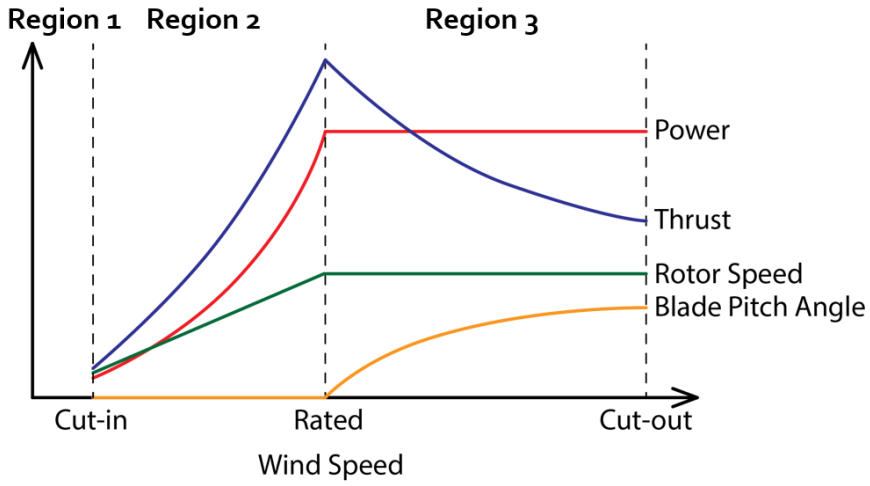

Figure 1.3. Wind turbine operating regions.

1.2.2 Structural Control

Structural control technology has been used to mitigate vibrations in buildings for decades [19]. At its most basic, this involves mounting a tuned mass damper or similar device inside a structure to dissipate energy. This idea has been more recently been applied to floating wind turbines, having advantages over blade pitch control in that structural control works while the turbine is parked during extreme weather events or during maintenance.

Several modeling tools have been developed to support these endeavors. Lackner and Rotea [20] developed a modified version of FAST, known as FAST-SC, to incorporate two independent, orthogonal TMDs mounted to the nacelle. Semi-active and active control approaches are accomodated by allowing stiffness and damping to be dictated through Simulink. Another model, developed by Si, Karimi, and Gao [21], couples surge, pitch, and heave motions for a spar platform with a TMD installed in the hull. Locating structural

control devices in the hull of the platform is advantageous because they are located near the wave forcing on the structure.

With these and other modeling tools, multiple variations on the traditional TMD have been examined for application to FOWTs. In the work of Park et. al [22], nacelle-mounted passive and semi-active magnetorheological TMDs are applied to a monopile turbine and a tension leg platform (TLP), with the semiactive dampers using ground hook control. Both control schemes were found to reduce structural responses, with tower base ultimate loads on the TLP reduced by 9% using the semi-active dampers. Li and Gao [23] investigated the use of active hull-mounted TMDs using generalized H_∞ control on a barge-type FOWT. The damper controller is tuned using a reduced-order linear model. The active TMDs were found to reduce fatigue loads and generator power variation, but as applied did not work for extreme environments. Nacelle-mounted hybrid mass dampers are explored in the work of Hu and He [24]. A hybrid mass damper consists of a passive TMD with an actuator attached, in line with the spring and dashpot. The dampers, controlled by an LQR, were applied to a barge-type FOWT and found to reduce tower fore-aft loads by up to 60.7% in simulations.

A variation on the TMD setup, known as a ducted fluid absorber (DFA), has recently been developed that utilizes ballast seawater in the hull of the platform. This is an advantage over traditional TMDs, which require their own dedicated, typically solid mass. DFAs are also advantageous in that they have adjustable damping and stiffness based on orifice size and air pressure in their ductwork, so they can be tuned to different sea states. These dampers have been shown in simulations and scale model tests to reduce platform heave motion in FOWTs [25]. In this new work, the feasibility of dynamically adjusting the damper parameters to changing sea states is evaluated and confirmed, and a control law to make these adjustments is developed.

1.3 Contributions

Several contributions are made to the literature by this thesis and the associated published works [26–28], as follows:

- A generic blade pitch controller gain scheduling method for floating offshore wind turbines is developed based on nacelle velocity feedback and a two degree-of-freedom (DoF) model that captures the coupled response of the rotor angular motion and the primary platform rigid-body mode. A proportional gain on the nacelle velocity feedback signal is introduced and tuned using the two-DoF model such that a specified increase in damping of the rigid-body mode is achieved. The developed controller is evaluated for several floating platforms in multiple environmental conditions spanning region 3.

- The feasibility of using hull-based ducted fluid absorbers for vibration mitigation is examined. A cost function is chosen to optimize performance, and then a spectrum of damper settings are evaluated against it for a range of environmental conditions. A lookup table of best-performing damper settings, scheduled to sea state, is thus created. The lookup table is compared to 18.4 years of wave buoy data, and an optimal configuration is assigned to each point in time. By calculating the work done to increase damper pressure between subsequent time steps, the power consumption of the dampers is obtained.

- A control scheme to adjust the properties of ducted fluid absorbers based on the sea state is developed by coupling the aforementioned lookup table of optimal settings to a sea-state estimator. The resulting controller has subsequently been evaluated in time domain simulations.

A visual representation of where devices affected by this research are located on a floating wind turbine is depicted in Figure 1.4. The gain scheduling method developed

using the two-DoF model is applied to the blade pitch controller in the nacelle of the turbine. Several ducted fluid absorbers or other tunable TMDs can be positioned throughout the hull. Both of these mechanisms can be applied to minimize the vibration of the floating system.

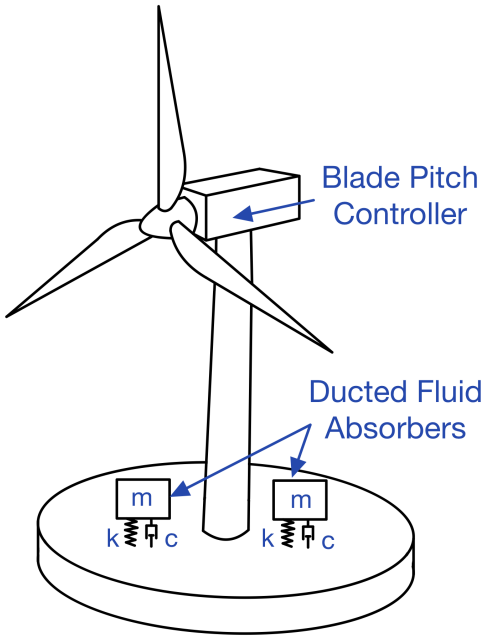

Figure 1.4. Approximation of the locations of the blade pitch controller and ducted fluid absorbers on a floating wind turbine.

CHAPTER 2

BLADE PITCH CONTROL

In this work, a tuning methodology for a basic collective blade pitch wind turbine controller employing tower-top feedback in region 3 is proposed for use in floating wind turbines with compliant foundations. The controller architecture is identical to that presented in [3], albeit, the tower-top feedback gain is scheduled with blade pitch angle instead of being constant. The generator torque is held constant. For the proposed tuning strategy, a two-DoF model is developed that is used to inform the scheduling of the controller gains. This is done to achieve rotor speed control similar to land-based turbines without significantly increasing blade pitch actuation motion, while simultaneously reducing platform pitch motion compared to other basic floating offshore wind turbine control tuning strategies like those employed in [29]. The model considers only the rotor angular motion (ϕ) and platform pitch angular motion (θ), as shown in Figure 2.1, as these are the DoF most strongly influenced by the collective blade pitch controller actions. The equations of motion for the two DoF are derived in a similar manner to that found in [30] for the rotor angular motion and [3] for the platform pitch motion. However, all terms that couple the DoF are retained in order to develop a more robust model that provides better

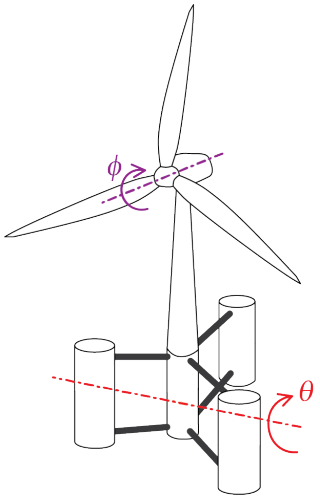

Figure 2.1. Degrees of freedom in controller tuning model

predictions of floating wind turbine behavior, and hence, a better tool for use in scheduling controller gains to achieve improved floating wind turbine performance. Much of this work is summarized in [26] and [27], but it is reiterated and expanded upon here.

2.1 Methods

To develop the gain tuning approach, the two-DoF model is defined for pitch and surge dominant rigid-body modes. Equations for determining the proportional and integral controller gains are defined, and then the two-DoF model is used to schedule an additional proportional feedback gain based on the fore-aft nacelle velocity. The developed controllers are then compared against several baselines for a semisubmersible, spar, and TLP platform in several operational environments.

2.1.1 Two Degree-of-Freedom Model

To begin, the angular equation of motion for the drivetrain about the low-speed shaft is written as

$$I_{drive}\frac{d}{dt}(\Omega_0 + d\Omega) = I_{drive}d\dot{\Omega} = Q_{aero} - Q_{gen,lss}, \tag{2.1}$$

where the low-speed shaft angular velocity Ω is equivalent to $d\phi/dt$, $d\Omega$ is a small deviation in this value, Ω_0 is the rated angular velocity, and other terms are defined in the nomenclature. The aerodynamic torque is a function of blade pitch and rotor speed, as noted by Jonkman [30]. Linearizing about the operating point yields

$$I_{drive}d\dot{\Omega} = Q_{aero} - Q_{gen,lss} \cong Q_0 + \frac{\partial Q}{\partial \Omega}d\Omega + \frac{\partial Q}{\partial \beta}d\beta + \frac{\partial Q}{\partial v}(dv - \dot{x}) - Q_{gen,lss}, \tag{2.2}$$

where Q_0 is the mean aerodynamic torque at the operating point and the partial derivatives represent the sensitivity of the aerodynamic torque to changes in rotor angular velocity, blade pitch angle and wind speed. The sensitivity of the aerodynamic torque to a change in wind speed is multiplied not only by a change in wind speed dv, but also by the apparent wind speed due to the tower-top's own velocity, $\dot{x}$. The platform pitch angle is

assumed to be small when determining $\dot{x}$. Noting that the mean aerodynamic torque is equal to the generator torque, which is taken as constant in region 3 here, gives

$$I_{drive}d\dot{\Omega} \cong \frac{\partial Q}{\partial \Omega}d\Omega + \frac{\partial Q}{\partial \beta}d\beta + \frac{\partial Q}{\partial v}(dv - \dot{x}). \tag{2.3}$$

The following sensitivity quantities are defined,

$$A_\Omega = \frac{\partial Q}{\partial \Omega}, A_\beta = \frac{\partial Q}{\partial \beta}, A_v = \frac{\partial Q}{\partial v}, \tag{2.4}$$

to be evaluated at the operating point. The definitions are then substituted into Eq. 2.3 to yield

$$I_{drive}d\dot{\Omega} \cong A_\Omega d\Omega + A_\beta d\beta + A_v(dv - \dot{x}). \tag{2.5}$$

The platform pitch equation of motion in the absence of wave forcing is written as

$$\overline{I}_{FOWT}\ddot{\theta} + \overline{C}_{FOWT}\dot{\theta} + \overline{K}_{FOWT}\theta = T_{aero}L_{hh}. \tag{2.6}$$

Note that the equations of motion are written about the point on the structure at which there is no mass/inertia coupling (inclusive of added mass and inertia). The hydrostatic stiffness employed includes both hydrostatic and mooring stiffnesses, and is selected to produce the correct platform pitch natural frequency. To continue, the tower-top fore-aft displacement and platform angular displacement are related as

$$x = L_{hh}\theta, \tag{2.7}$$

which, when substituted into Eq. 2.6, yields

$$\frac{\overline{I}_{FOWT}}{L_{hh}^2}\ddot{x} + \frac{\overline{C}_{FOWT}}{L_{hh}^2}\dot{x} + \frac{\overline{K}_{FOWT}}{L_{hh}^2}x = T_{aero}. \tag{2.8}$$

Defining the following FOWT properties

$$I_{FOWT} = \frac{\overline{I}_{FOWT}}{L_{hh}^2}, C_{FOWT} = \frac{\overline{C}_{FOWT}}{L_{hh}^2}, K_{FOWT} = \frac{\overline{K}_{FOWT}}{L_{hh}^2}, \tag{2.9}$$

and substituting the three quantities into Eq. 2.8 gives

$$I_{FOWT}\ddot{x} + C_{FOWT}\dot{x} + K_{FOWT}x = T_{aero}. \tag{2.10}$$

Linearizing the aerodynamic thrust about the operating point gives

$$I_{FOWT}\ddot{x} + C_{FOWT}\dot{x} + K_{FOWT}x = T_{aero} \cong T_0 + \frac{\partial T}{\partial \Omega}d\Omega + \frac{\partial T}{\partial \beta}d\beta + \frac{\partial T}{\partial v}(dv - \dot{x}), \tag{2.11}$$

which upon utilization of the following thrust sensitivity definitions

$$B_\Omega = \frac{\partial T}{\partial \Omega}, B_\beta = \frac{\partial T}{\partial \beta}, B_v = \frac{\partial T}{\partial v}, \tag{2.12}$$

yields

$$I_{FOWT}\ddot{x} + C_{FOWT}\dot{x} + K_{FOWT}x \cong T_0 + B_\Omega d\Omega + B_\beta d\beta + B_v(dv - \dot{x}). \tag{2.13}$$

To eliminate the mean thrust at the operating point, the tower-top motion about the static equilibrium position due to the thrust T_0 is defined as

$$y = x - \frac{T_0}{K_{FOWT}}. \tag{2.14}$$

Substitution of Eq. 2.14 into Eq. 2.13 results in

$$I_{FOWT}\ddot{y} + C_{FOWT}\dot{y} + K_{FOWT}y \cong B_\Omega d\Omega + B_\beta d\beta + B_v(dv - \dot{y}). \tag{2.15}$$

The controller gains contribute to the desired change in blade pitch angle $d\beta$ through the relationship

$$d\beta = k_p d\Omega + k_i \int_0^t d\Omega dt + k_{px}\dot{x}. \tag{2.16}$$

This control equation consists of a standard proportional-integral controller targeting rotor speed error $d\Omega$ and is supplemented with an additional term proportional to the tower-top fore-aft velocity. Noting that the rotor angular displacement and angular velocity are related as

$$\dot{\phi} = d\Omega, \tag{2.17}$$

and substituting the control equation into Eq. 2.5, the drivetrain angular equation of motion, gives

$$I_{drive}\ddot{\phi} - (A_\Omega + A_\beta k_p)\dot{\phi} - A_\beta k_i \phi + (A_v - A_\beta k_{px})\dot{x} \cong A_v dv. \tag{2.18}$$

Substitution of the control equation into the platform pitch equation, Eq. 2.15, yields

$$I_{FOWT}\ddot{y} + (C_{FOWT} + B_v - B_\beta k_{px})\dot{y} + K_{FOWT}y - (B_\Omega + B_\beta k_p)\dot{\phi} - B_\beta k_i \phi \cong B_v dv. \quad (2.19)$$

Representing Eq. 2.18 and Eq. 2.19 in matrix equation form yields the following two-DoF coupled equations of motion,

$$\begin{bmatrix} I_{FOWT} & 0 \\ 0 & I_{drive} \end{bmatrix} \begin{Bmatrix} \ddot{y} \\ \ddot{\phi} \end{Bmatrix} + \begin{bmatrix} (C_{FOWT} + B_v - B_\beta k_{px}) & -(B_\Omega + B_\beta k_p) \\ (A_v - A_\beta k_{px}) & -(A_\Omega + A_\beta k_p) \end{bmatrix} \begin{Bmatrix} \dot{y} \\ \dot{\phi} \end{Bmatrix} + \begin{bmatrix} K_{FOWT} & -B_\beta k_i \\ 0 & -A_\beta k_i \end{bmatrix} \begin{Bmatrix} y \\ \phi \end{Bmatrix} = \begin{Bmatrix} B_v \\ A_v \end{Bmatrix} dv. \quad (2.20)$$

The natural frequencies and damping ratios can be obtained from the two-DoF model by first considering the free vibration problem, which has the form

$$\begin{bmatrix} I_{FOWT} & 0 \\ 0 & I_{drive} \end{bmatrix} \begin{Bmatrix} \ddot{y} \\ \ddot{\phi} \end{Bmatrix} + \begin{bmatrix} (C_{FOWT} + B_v - B_\beta k_{px}) & -(B_\Omega + B_\beta k_p) \\ (A_v - A_\beta k_{px}) & -(A_\Omega + A_\beta k_p) \end{bmatrix} \begin{Bmatrix} \dot{y} \\ \dot{\phi} \end{Bmatrix} + \begin{bmatrix} K_{FOWT} & -B_\beta k_i \\ 0 & -A_\beta k_i \end{bmatrix} \begin{Bmatrix} y \\ \phi \end{Bmatrix} = \begin{Bmatrix} 0 \\ 0 \end{Bmatrix}. \quad (2.21)$$

Next, the following assumptions are made for the solutions of the tower-top fore-aft and rotor angular motions [31],

$$\begin{Bmatrix} y(t) \\ \phi(t) \end{Bmatrix} = \begin{Bmatrix} Y \\ \Phi \end{Bmatrix} e^{st}, \quad (2.22)$$

where Y, Φ, and s are constants. Substitution of Eq. 2.22 into Eq. 2.21 gives

$$\begin{bmatrix} s^2R_{11} + sR_{12} + R_{13} & sR_{21} - R_{22} \\ sR_{31} & s^2R_{41} + sR_{42} - R_{43} \end{bmatrix} \begin{Bmatrix} Y \\ \Phi \end{Bmatrix} \cong \begin{Bmatrix} 0 \\ 0 \end{Bmatrix}$$

$$\begin{aligned} R_{11} &= I_{FOWT} \\ R_{12} &= C_{FOWT} + B_v - B_\beta k_{px} \\ R_{13} &= K_{FOWT} \\ R_{21} &= -B_\Omega - B_\beta k_{px} \\ R_{22} &= -B_\beta k_i \\ R_{31} &= A_v - A_\beta k_p x \\ R_{41} &= I_{drive} \\ R_{42} &= -A_\Omega - A_\beta k_p \\ R_{43} &= -A_\beta k_i \end{aligned} \tag{2.23}$$

The determinant of the 2×2 coefficient matrix of Eq. 2.23 is set to zero, which yields a characteristic equation of the form

$$(s - s_1)(s - s_2)(s - s_3)(s - s_4) = 0, \tag{2.24}$$

where s_1, s_2, s_3, and s_4 are the four roots of the characteristic equation. These four roots also constitute the system poles [32], two predominantly associated with the platform angular motion DoF and the other two primarily associated with the rotor angular motion DoF. These poles can be used to determine estimates for the natural frequencies and damping ratios for the rotor angular and platform pitch motions [33].

2.1.2 Modeling the TLP

For TLPs, there is little to no platform pitch motion. Instead, the DoF most susceptible to instability due to wind forcing is platform surge. Because of this, the surge degree of freedom (equivalent to the tower-top displacement degree of freedom, x) is used in place of platform pitch to adapt the two-DoF model for use with a TLP. This is shown in Figure

2.2. In addition, $\overline{I}_{FOWT}$ is recast to M_{FOWT}, and $\overline{C}_{FOWT}$ and $\overline{K}_{FOWT}$ are specified with respect to linear surge motion rather than rotational pitch. As such, Eq. 2.21 becomes

$$\begin{bmatrix} M_{FOWT} & 0 \\ 0 & I_{drive} \end{bmatrix} \begin{Bmatrix} \ddot{x} \\ \ddot{\phi} \end{Bmatrix} + \begin{bmatrix} (C_{FOWT} + B_v - B_\beta k_{px}) & -(B_\Omega + B_\beta k_p) \\ (A_v - A_\beta k_{px}) & -(A_\Omega + A_\beta k_p) \end{bmatrix} \begin{Bmatrix} \dot{x} \\ \dot{\phi} \end{Bmatrix} + \begin{bmatrix} K_{FOWT} & -B_\beta k_i \\ 0 & -A_\beta k_i \end{bmatrix} \begin{Bmatrix} x \\ \phi \end{Bmatrix} = \begin{Bmatrix} 0 \\ 0 \end{Bmatrix} \tag{2.25}$$

and these changes are carried through to subsequent steps of the solution.

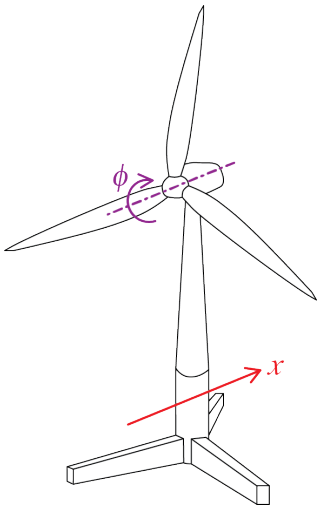

Figure 2.2. Degrees of freedom in controller tuning model for the TLP

2.1.3 Scheduling of Controller Gains

In this section, the simplistic approach with which the collective blade pitch wind turbine controller gains are scheduled with blade pitch angle is presented. To begin, the proportional and integral gains are tuned in a manner similar to the NREL ROSCO controller [18]. The proportional gain k_p and integral gain k_i are determined as

$$\begin{aligned} k_p &= -2A_\beta^{-1}(A_\Omega + I_{drive}\zeta_{rot,des}\omega_{n,rot,des}) \\ k_i &= -A_\beta^{-1} I_{drive}\omega_{n,rot,des}^2 \end{aligned} \tag{2.26}$$

where $\omega_{n,rot,des}$ and $\zeta_{rot,des}$ are the controller design natural frequency and design damping ratio for the rotor angular motion. Previous work by Jonkman [30] found a controller frequency of 0.6 rad/s and a design damping ratio of 0.7 to work well for a turbine of this size. For the current work, $\omega_{n,rot,des}$ was set to 0.6 rad/s and $\zeta_{rot,des}$ was 1.0. The higher design damping ratio accounts for an additional aerodynamic damping term A_Ω being added to the equation for k_p.

The aerodynamic sensitivities required for scheduling the gains are obtained from linearization analyses in OpenFAST [34]. The aerodynamic sensitivities vary with the wind speed, and hence the corresponding blade pitch angle. The linearization analyses are conducted for several wind speeds ranging from rated wind speed to cut-out wind speed, and the obtained sensitivities are smoothed using a quadratic polynomial fit prior to insertion into Eq. 2.26 for determining the gain schedules. This produces a smooth set of control gain schedules for use in the wind turbine controller. The frozen wake assumption is used in these analyses.

With the proportional and integral gains determined, the remaining tower-top feedback gain k_{px} is scheduled by utilizing the previously described two-DoF model. For a given wind speed with the associated aerodynamic sensitivities and associated gains k_p and k_i, the gain k_{px} is solved for such that a specified increase in the platform pitch damping, $\Delta\zeta_{DoF}$, is achieved over the case where $k_{px} = 0$. This is repeated multiple times across the range of wind speeds in region 3, from rated to cut-out, in order to determine the scheduling of the gain k_{px}. As is done in the first step of this tuning procedure, all aerodynamic sensitivities used are determined from OpenFAST linearization analyses and smoothed with a quadratic polynomial fit prior to use in the two-DoF model. It should be noted that there is a limit to the increase in platform damping that can be achieved using active blade pitch control, and as such, it is suggested that modest values of $\Delta\zeta_{DoF}$ be used to achieve reasonable results. Experience has shown values of $\Delta\zeta_{DoF}$ of 0.05 or less to work well.

To complete the controller, which is implemented using the MATLAB Simulink option in OpenFAST, the tower-top fore-aft velocity signal is filtered to isolate the motion near the platform pitch natural frequency for use in the controller. A second-order band-pass filter is implemented as per [35], the transfer function of which is described as

$$H(s) = \frac{(2\Delta\omega)s}{s^2 + (2\Delta\omega)s + \omega_{n,DoF}^2}, \tag{2.27}$$

where $\Delta\omega$ is a deviation from the pitch natural frequency where the signal will be reduced by three decibels and $\omega_{n,DoF}$ is the platform natural frequency in pitch (for the semisubmersible and spar) or surge (for the TLP).

Several baseline controllers were also tested for comparison. A case where $\Delta\zeta_{DoF} = 0$ is representative of a conventional wind turbine controller mounted to a floating platform. This controller is also tested for the case where all rigid body platform modes are locked, to represent a turbine on land. To examine performance relative to another common method of overcoming the negative damping problem, the detuned controller developed by Jonkman [3] is tested using a $\omega_{n,rot,des}$ of 0.2 rad/s for the semisubmersible and spar demonstration systems and 0.15 rad/s for the TLP. These values are chosen such that they are slower than the natural frequency of the dominant rigid-body mode of each platform (pitch for the semisubmersible and spar, surge for the TLP). By doing this, the controller can no longer react fast enough to excite these dominant rigid-body modes.

2.1.4 Demonstration Systems

The DeepCwind OC4 semisubmersible, OC3 Hywind spar, and DeepCwind TLP are studied here, chosen based on the accessibility of their specifications and to represent common offshore wind platforms. Definitions required for modeling the semisubmersible in OpenFAST can be found in [29], while the spar platform is specified in [36] and the TLP in [37]. Models of these floating systems are shown in Figure 2.3.

Specifications pertinent to controller development using the two-DoF models are given in Table 2.1. It should be noted that both physical and added inertia are included in

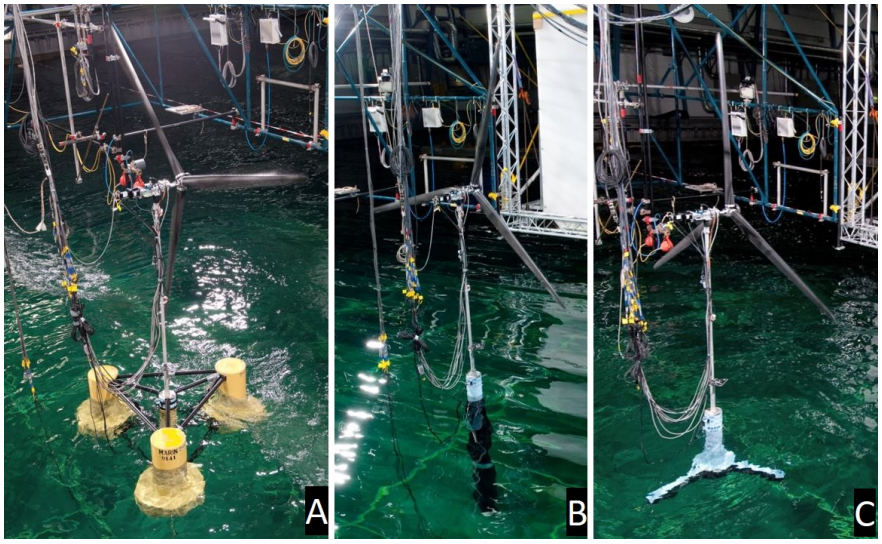

Figure 2.3. Semisubmersible (A), spar-buoy (B), and TLP (C) platform scale models

Table 2.1. Two-DoF model inputs

Quantity	Semisubmersible	Spar	TLP
$\overline{I}_{FOWT}/M_{FOWT}$	1.75×10^{10} kg m^2	2.61×10^{10} kg m^2	3.57×10^{6} kg
$\overline{C}_{FOWT}$	4.35×10^{8} N m s/rad	5.80×10^{8} N m s/rad	5.61×10^{4} N s/m
$\overline{K}_{FOWT}$	1.08×10^{9} N m/rad	1.29×10^{9} N m/rad	8.81×10^{4} N/m
L_{hh} m	100.9	160.5	1†
I_{drive} kg m^2	4.38×10^{7}	4.38×10^{7}	4.38×10^{7}

† Unity, because there is no rotational coupling for the TLP.

$\overline{I}_{FOWT}/M_{FOWT}$ and that the values correspond with the location at which surge and pitch motions uncouple. The platform rotational stiffness is selected to give the correct platform pitch natural frequency as computed from a full OpenFAST simulation, and the linearized platform hydrodynamic damping is assumed to be 5% of critical (which is reasonable based on DeepCwind test data [38]). The hub height parameter, L_{hh}, is measured upward from this location. All of these platforms use the NREL-5MW wind turbine described in [34]. Some basic properties of this wind turbine are given in Table 2.2.

The nacelle velocity feedback filter for each system was centered around the dominant rigid-body natural frequency, $\omega_{n.DoF}$ (pitch for the semisubersible and spar, surge for the TLP). Values of approximately 40% of $\omega_{n.DoF}$ were found to produce good results for the filter width, $\Delta\omega$. These filter parameters are outlined in Table 2.3.

Table 2.2. Properties of the NREL 5MW wind turbine

Property	Value
Power rating	5 MW
Rotor diameter	126 m
Rated wind speed	11.4 m/s
Rated rotor speed	12.1 rpm
Rotor mass	110000 kg
Nacelle mass	240000 kg
Tower mass	347460 kg

Table 2.3. Nacelle velocity feedback filter parameters

Quantity	Semisubmersible	Spar	TLP
$\omega_{n.DoF}$ rad/s	0.237	0.210	0.157
$\Delta\omega$ rad/s	0.094	0.075	0.063

2.1.5 Simulation Environments

The environmental conditions used in full time-domain OpenFAST simulations are outlined in Table 2.4. These conditions were modeled after IEC DLC 1.2 for the Gulf of

Table 2.4. Simulated Environmental Conditions

Mean wind speed (m/s)	Significant wave height (m)	Peak wave period (s)	JONSWAP gamma
12	1.21	7.30	1.6
18	2.05	8.12	1.7

Maine. All winds and waves were collinear with no current. The wind fields were generated in TurbSim using the Kaimal spectrum and a normal turbulence model with class A intensity. Eighteen random seeds of each load case were simulated, and 600 seconds of data were recorded after a 250-second lead-in time to eliminate transients. These test specifications follow from those outlined by the American Bureau of Shipping [39]. The twelve meter per second condition was selected because the platform pitch instability is most prominent just after rated wind speed [40]. The eighteen meter per second condition was selected as it is near the middle of region 3 for the NREL 5-MW wind turbine.

2.2 Results and Discussion

2.2.1 Torque and Thrust Sensitivities

Thrust (B) and torque (A) sensitivities to blate pitch β, rotor speed Ω, and wind speed v are shown in Figure 2.4. Data points from the linearization analyses in OpenFAST are shown along with quadratic fits of the data. The equations for the quadratic fits of the aerodynamic sensitivities are given in Table 2.5.

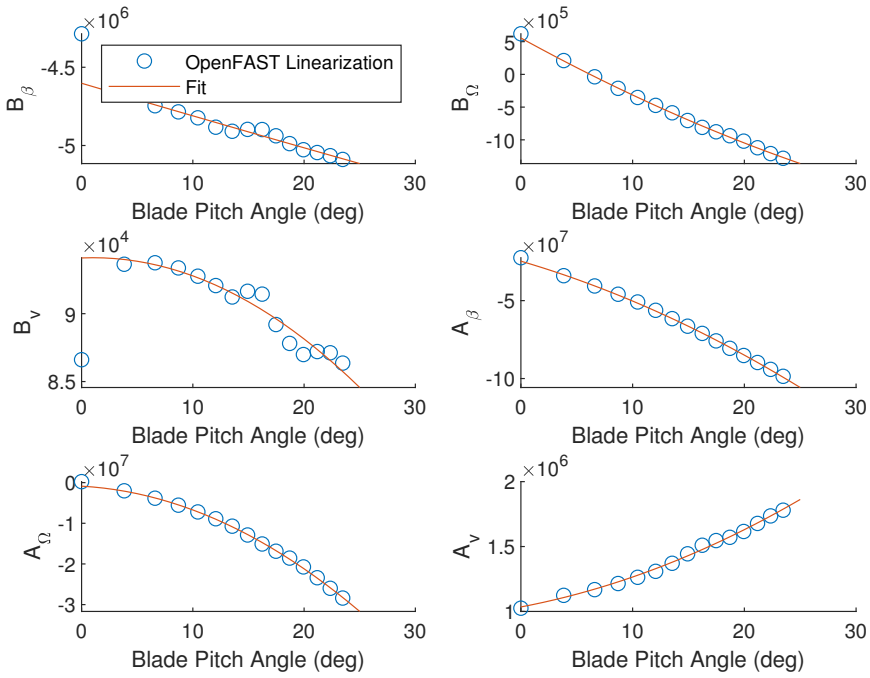

Figure 2.4. Thrust and torque sensitivities of the NREL 5MW at different blade pitch angles

Table 2.5. Quadratic fit of thrust and torque sensitivities

Sensitivity	Fit
B_β	$19.19\beta^2 - 2.101 \times 10^4\beta - 4.602 \times 10^6$
B_Ω	$690.1\beta^2 - 9.398 \times 10^4\beta + 5.556 \times 10^5$
B_v	$-16.65\beta^2 + 34.48\beta + 9.410 \times 10^4$
A_β	$-4.551 \times 10^4\beta^2 - 2.105 \times 10^6\beta - 2.467 \times 10^7$
A_Ω	$-4.316 \times 10^4\beta^2 - 1.531 \times 10^5\beta - 8.736 \times 10^5$
A_v	$670.0\beta^2 + 1.638 \times 10^4\beta + 1.034 \times 10^6$

2.2.2 Example Feedback Filter Results

In this subsection, an example implementation of the nacelle velocity feedback filter from Eq. 2.27 is shown as applied to the semisubmersible platform using the values prescribed by Table 2.3. A bode plot of this filter is shown in Figure 2.5. Unfiltered signal strength is unchanged at the target period, $\omega_{n,pit}$, but the signal strength of higher and lower frequencies is diminished by the filter. As can be seen in the example time domain results for a 12 m/s wind condition shown in Figure 2.6, the filter adequately reduces noise levels while maintaining the shape of signal trends.

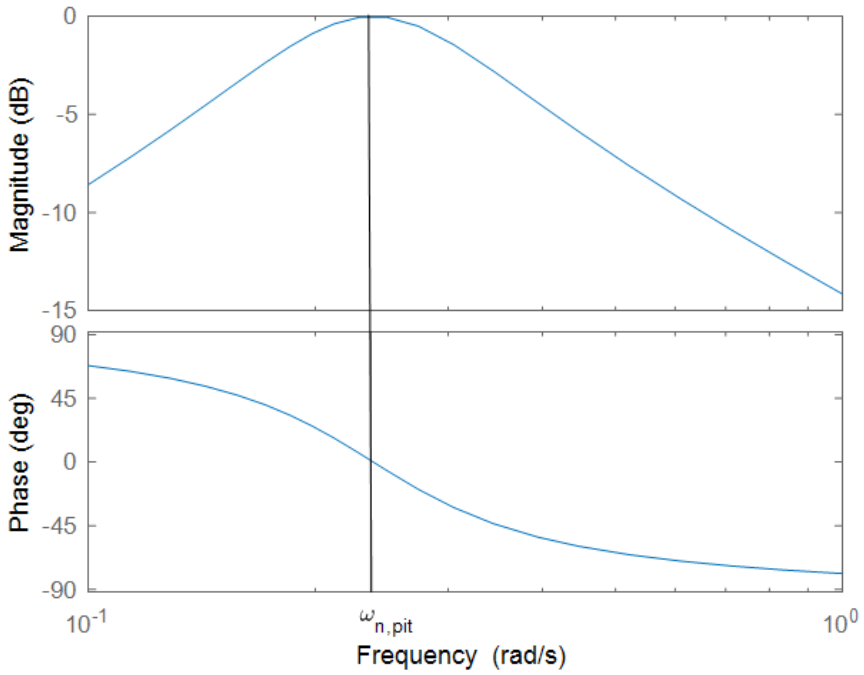

Figure 2.5. Nacelle velocity feedback filter bode plot

2.2.3 Gain Schedules

Gain schedules developed using the aforementioned methods for the OC4 Semisubmersible are shown in Figure 2.7. The k_p and k_i gains for all but the detuned ($\omega 0.2$) controller are identical, while k_{px} gains increase in magnitude from the 1.5% to the 4.5% controllers. The $\omega 0.2$ and 0% controllers both have k_{px} set to zero for the entire range of blade pitch angles.

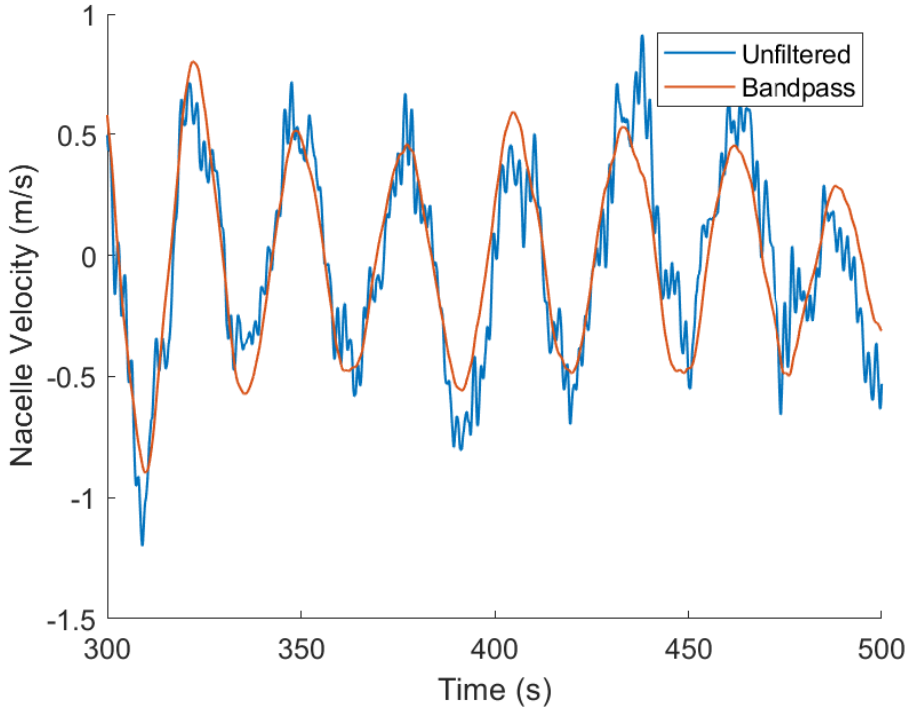

Figure 2.6. Example time domain filter data

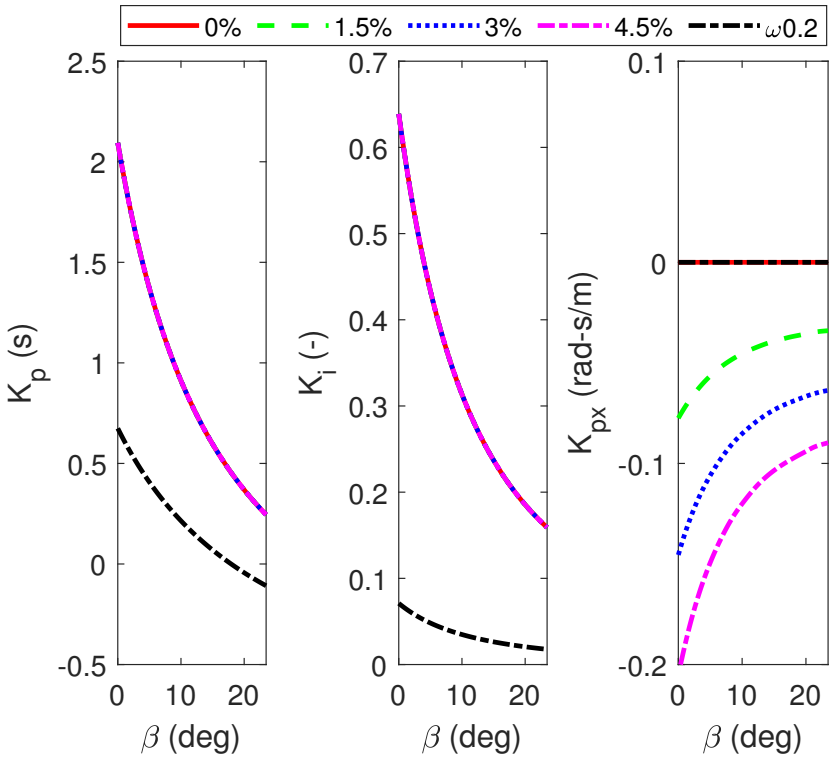

Figure 2.7. Gain schedules for the semisubmersible platform

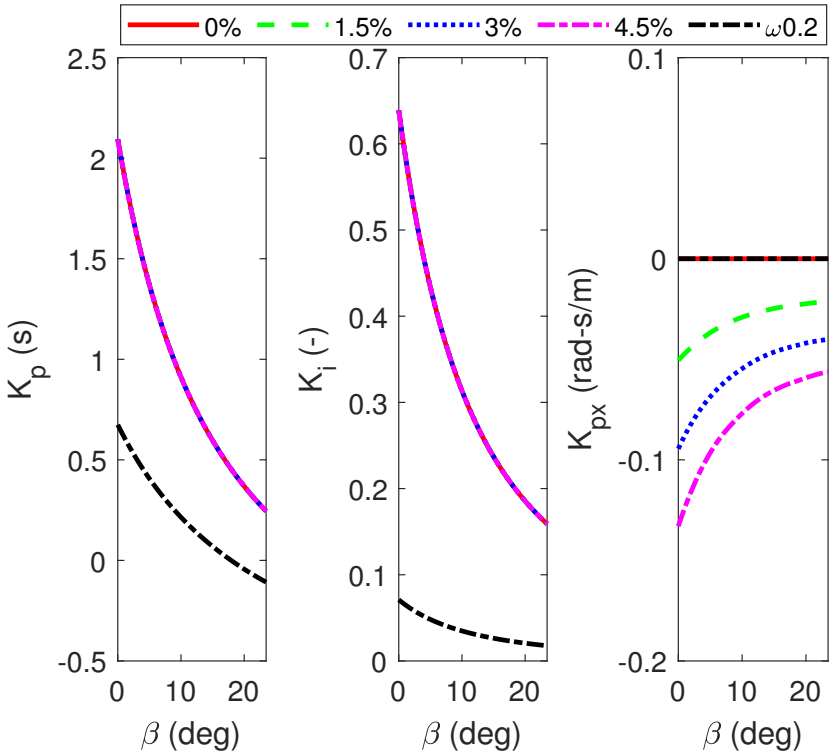

Figure 2.8. Gain schedules for the spar platform

Gain schedules for the OC3 Spar are presented in Figure 2.8. The k_p and k_i gains are scheduled identically to the semisubmersible, though k_{px} gains are smaller in magnitude for the same $\Delta\zeta_{DoF}$ and blade pitch angle.

The DeepCwind TLP's gain schedule is shown in Figure 2.9. The detuned controller natural frequency is lower for this platform than for the other two (labelled $\omega 0.15$, with a natural frequency of 0.15 rad/s). This is to put the controller natural frequency below the lowest rigid body frequency mode, which for the TLP is surge at 0.16 rad/s. Nacelle velocity feedback gains k_{px} for the two-DoF tuned controllers are larger in magnitude for the TLP than for either of the other platforms.

2.2.4 Performance Characteristics

Relative performance between controllers for varying systems and load cases are examined. In the following figures, the bar plots show average values for the selected metrics. The superimposed box plots show the median in red, 25th and 75th percentiles at

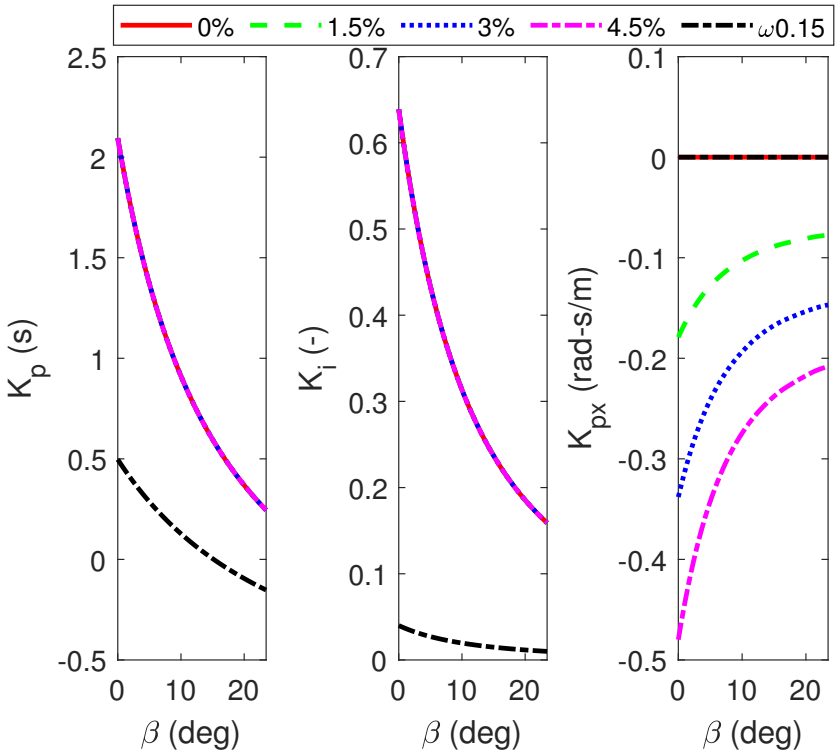

Figure 2.9. Gain schedules for the TLP

the bottom and top of the box, and extreme values at the ends of the whiskers. Where range is discussed, it refers to the difference between extreme values.

Of the controllers examined, the 0% controller is similar to the standard NREL wind turbine controller from [18], the 1.5%, 3.0%, and 4.5% controllers are tuned using the two-DoF model, and the $\omega 0.2$ and $\omega 0.15$ controllers represent the appropriate detuned controllers for the various hulls. The performance of the 0% controller mounted to a rigid foundation is included for reference in each of the following comparisons, labelled 'Land'.

From Figure 2.10, representing the OC4 semisubmersible for a 12-m/s average wind, it can be seen that the detuned controller results in the highest average power among the floating turbines, but also the most variation in power. Predictably, the fixed-base turbine produces the most power with the least variation. The two-DoF tuned controllers are largely on par with the 0% controller for this load case, with a slight reduction in platform pitching motion.

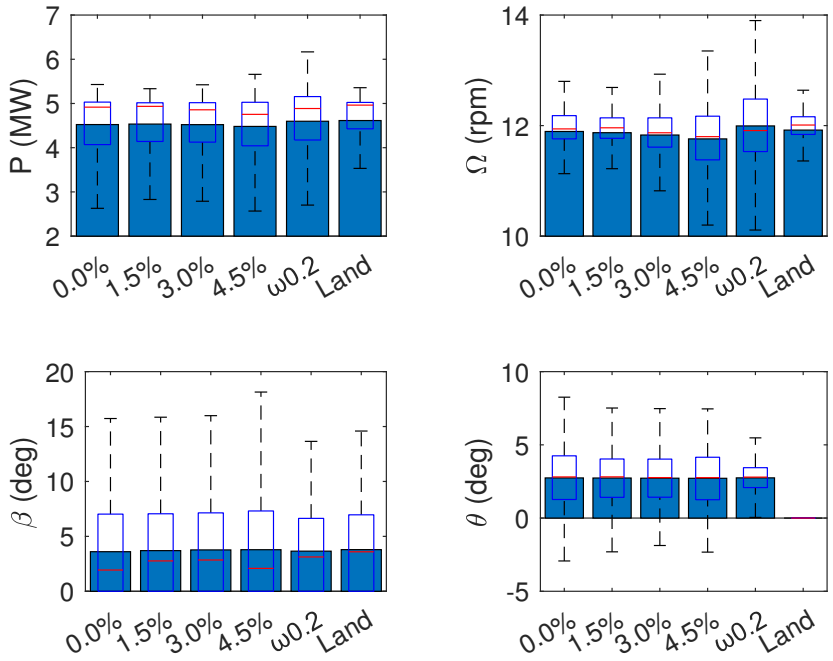

Figure 2.10. Semisubmersible performance metrics; 12-m/s wind case

Results for the 18-m/s load case, seen in Figure 2.11, show slightly different trends. Power range for the detuned controller is over twice that of any other tuning strategy. Average power, though, is much more even between the methods. Of interest, the platform pitching range of the two-DoF tuned controllers is more in line with the detuned controller than the 0% controller. Of the various $\Delta\zeta_x$ values examined, 1.5% provides the smallest range in power at the expense of a small increase in platform pitch motion.

The 12-m/s load case for the spar is shown in Figure 2.12. Power metrics for the two-DoF tuned controllers are largely on par with the 0% for this case, with some slight improvements. As with the semisubmersible results, the detuned controller and the fixed-base turbine result in the least range in blade pitch.

For the 18-m/s case depicted in Figure 2.13 for the spar, trends are largely the same as they were for the semisubmersible. Of the three two-DoF tuned controllers, 1.5% results in the least power range but the most blade pitch range and platform pitch range. More

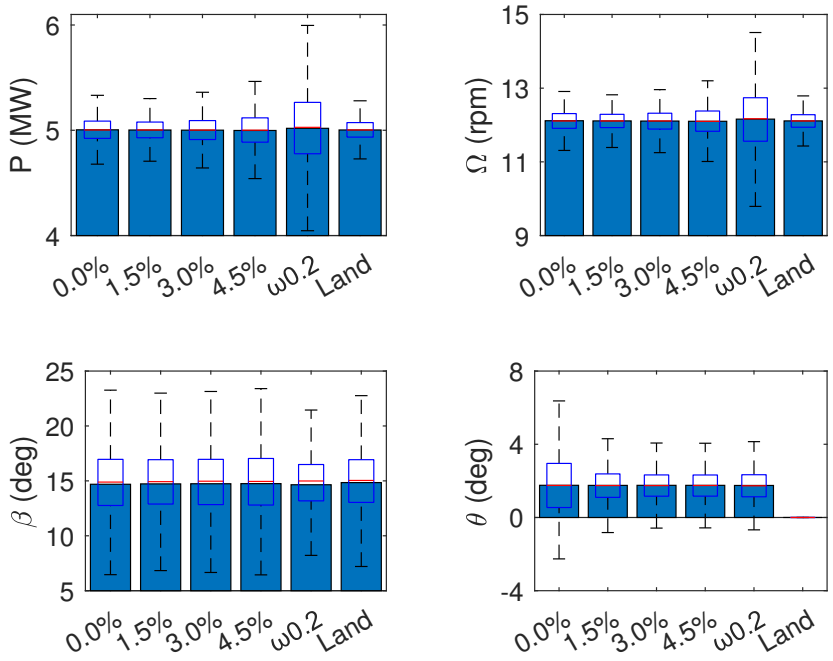

Figure 2.11. Semisubmersible performance metrics; 18-m/s wind case

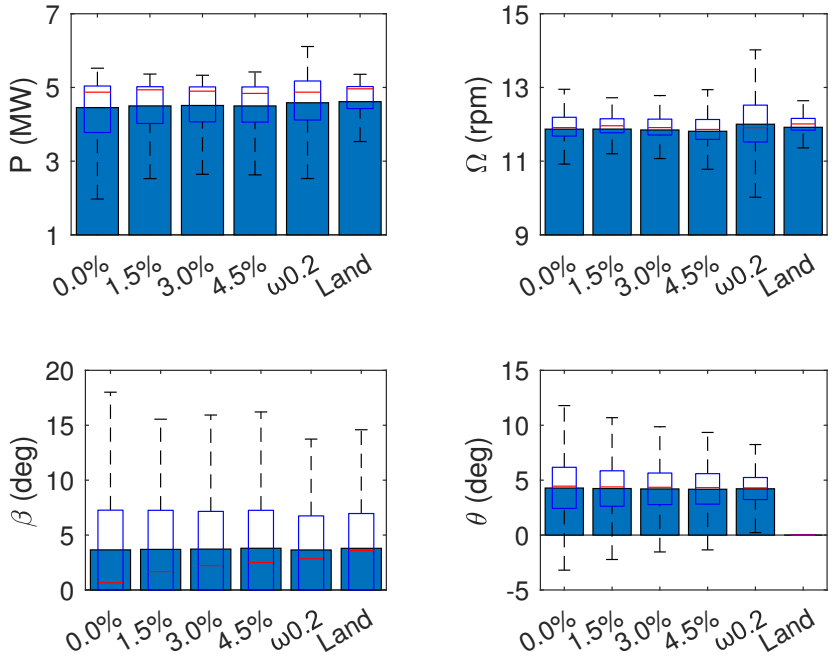

Figure 2.12. Spar performance metrics; 12-m/s wind case

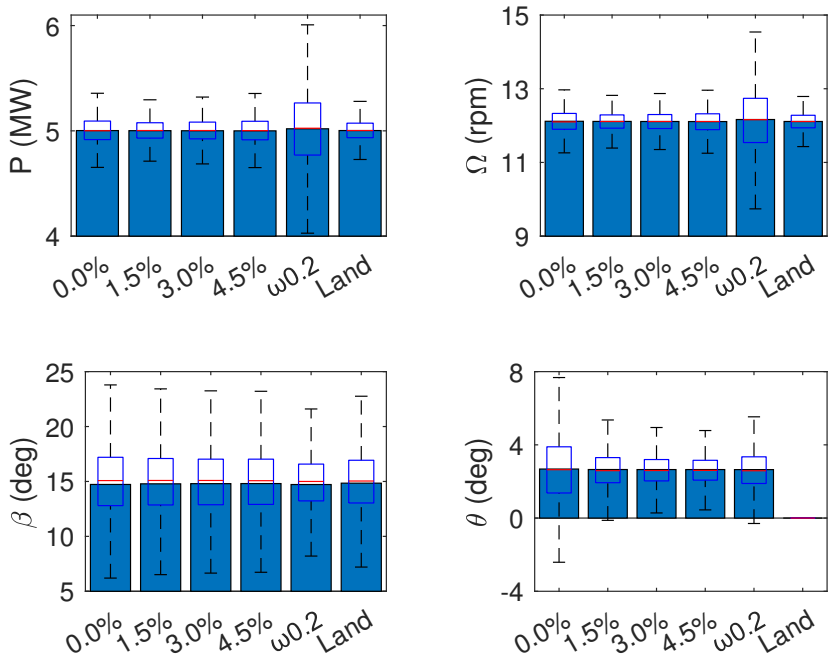

Figure 2.13. Spar performance metrics; 18-m/s wind case

importantly, the power metrics are similar to the land case with platform motions being as good or better than the detuned case all while requiring a only a small increase in blade pitch actuation duty.

For the TLP, it should be noted that the detuned controller is tuned to 0.15 rad/s versus 0.2 rad/s to accommodate its lower natural frequency for the primary rigid-body mode. It should also be noted that statistics for surge are presented instead of pitch, because that is the dominant mode.

For the 12-m/s case shown in Figure 2.14, the 4.5% controller provides the lowest average power of those tested while the 1.5% controller performs more on par with the traditional controllers. Surge range is decreased for the two-DoF controllers over the 0% case.

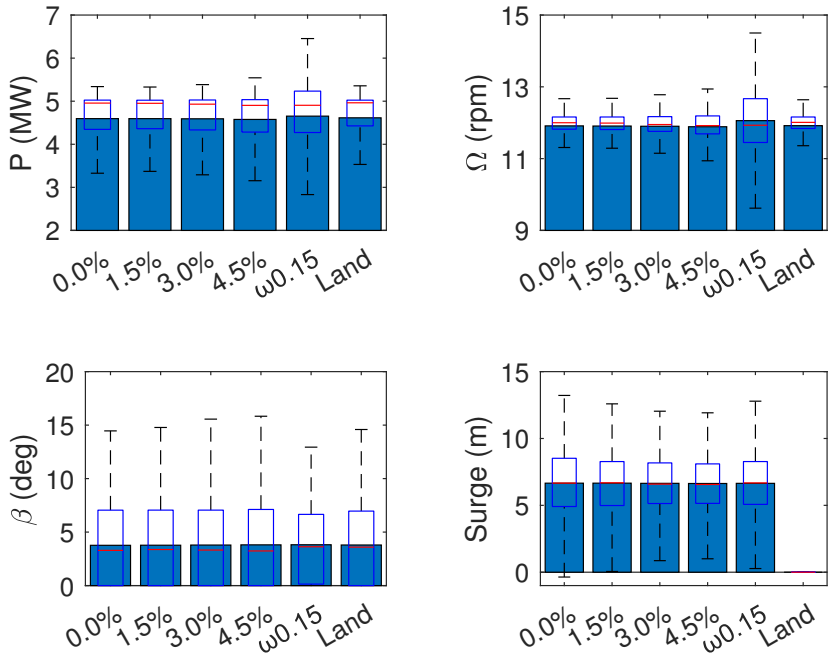

Figure 2.14. TLP performance metrics; 12-m/s wind case

In the 18-m/s case (Figure 2.15), power range for the detuned controller is over twice that of the 4.5% controller. The 4.5% controller returns slightly more power range than the 1.5% or 3.0% controllers, though it performs best at minimizing surge range.

2.2.5 Power Spectrum Response for Dominant Rigid Body Mode

In this section, power spectrum responses of the controllers for the dominant rigid-body mode of each platform are presented. The natural pitch/surge frequency for a parked turbine in still air is included for reference. For the OC4 Semisubmersible in 12 m/s mean wind (Figure 2.16), it can be seen that the two-DoF tuned controllers provide a middle ground between the detuned and the 0% controllers for platform pitching. Of interest, the peak response frequency can be shifted significantly by increasing the $\Delta\zeta_{DoF}$ value used (0.038 Hz for the 0% controller vs. 0.044 Hz for the 4.5%). Previous work has shown that the controller influenced the platform rigid-body natural frequencies [26], so this is to be expected.

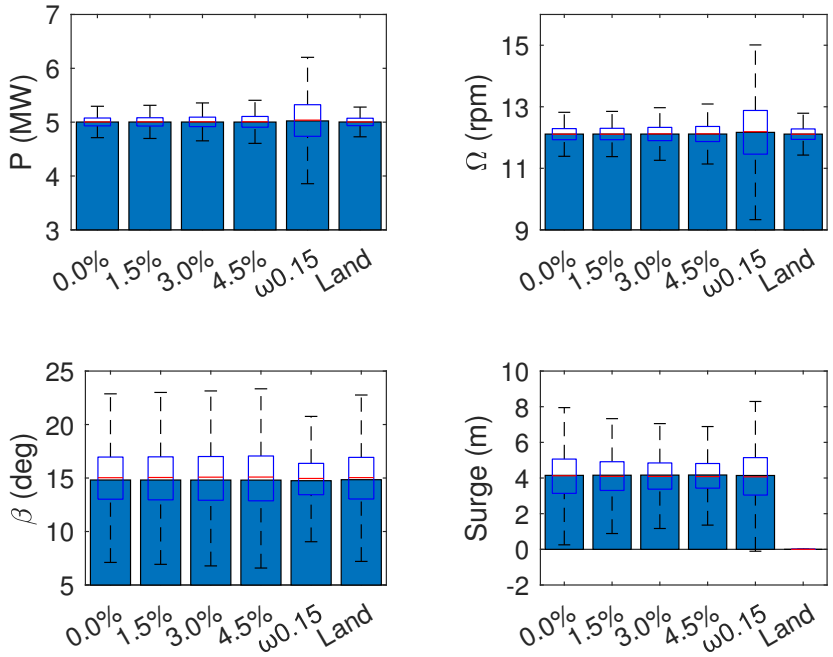

Figure 2.15. TLP performance metrics; 18-m/s wind case

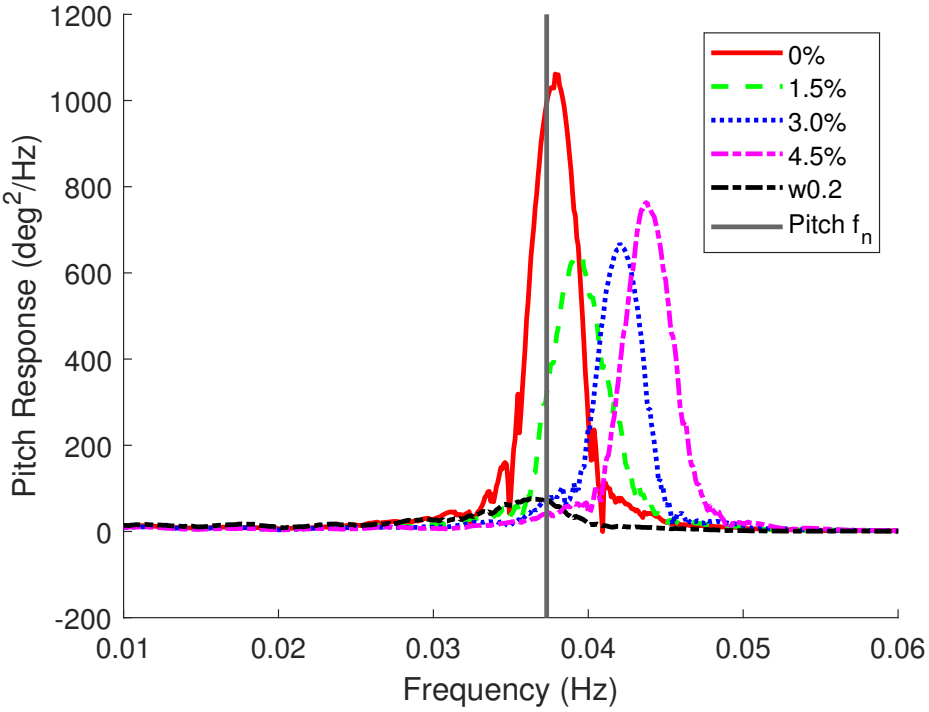

Figure 2.16. Semisubmersible platform pitch response, 12 m/s wind case

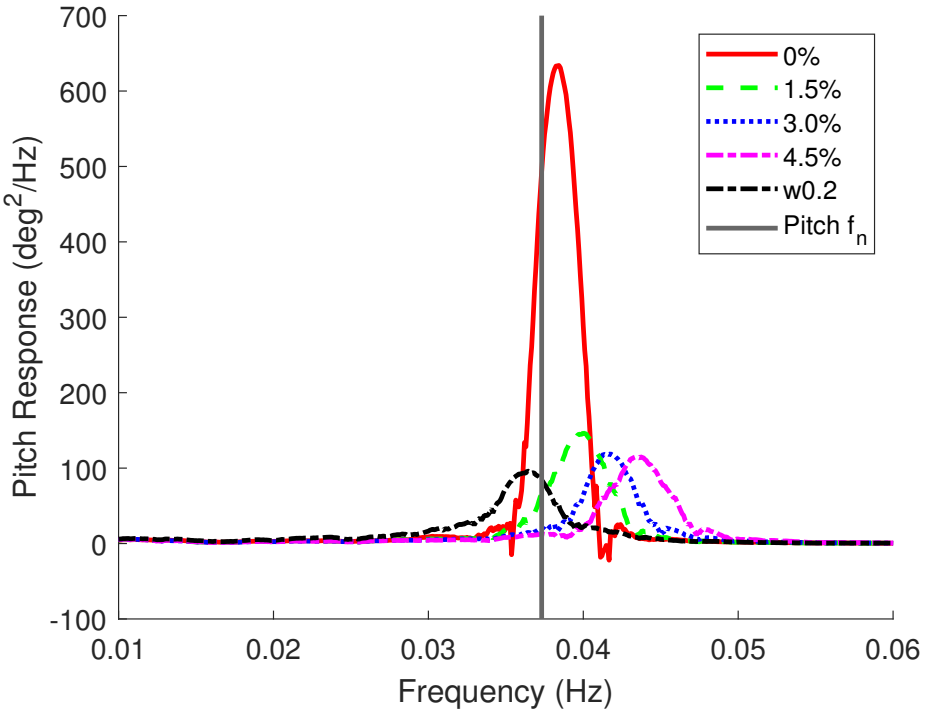

Figure 2.17. Semisubmersible platform pitch response, 18 m/s wind case

In the 18 m/s wind case shown in Figure 2.17, trends among the two-DoF tuned controllers are reversed from the 12 m/s case, with the 4.5% controller producing less response than the 3.0% or the 1.5%. All three of these controllers provide a response level much more akin to the detuned controller than the 0%. Trends in the peak response frequency carry over from the 12 m/s case.

The platform pitch response of the spar platform in the 12 m/s average wind case is shown in Figure 2.18. Interestingly, the 3.0% and 4.5% controllers perform better than the 1.5%, contrary to the results for the semisubmersible in this load case (Figure 2.16). However, the trend of peak response frequency increasing with increasing $\Delta\zeta_{DoF}$ is the same.

In the 18 m/s load case for the Spar, shown in Figure 2.19, trends are similar to those for the Semisubmersible in the same conditions. However, the 4.5% and 3.0% controllers produce less pitch response than the detuned controller.

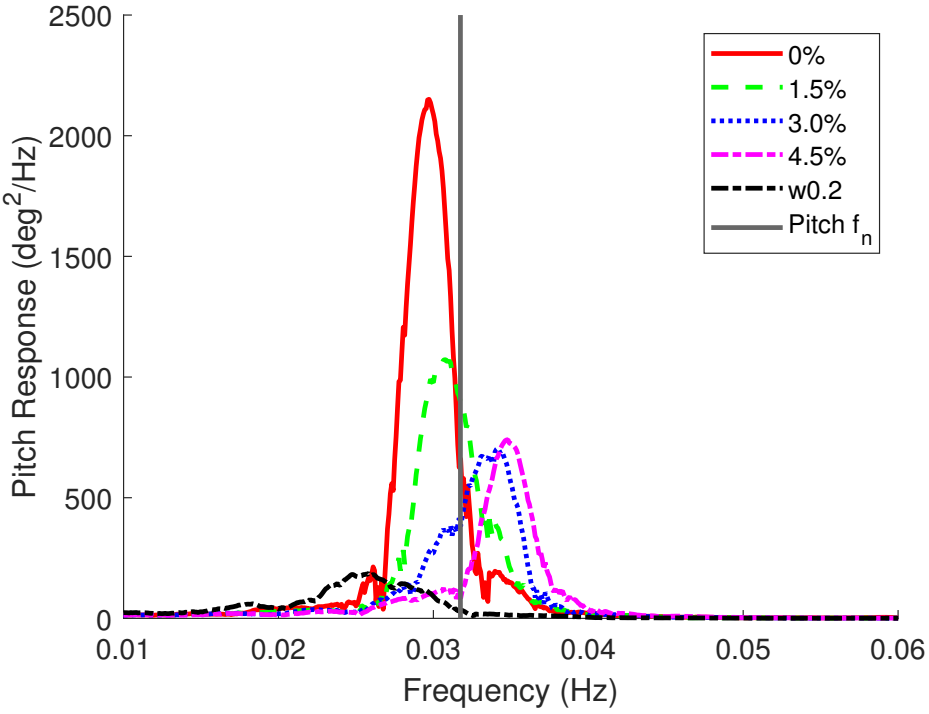

Figure 2.18. Spar platform pitch response, 12 m/s wind case

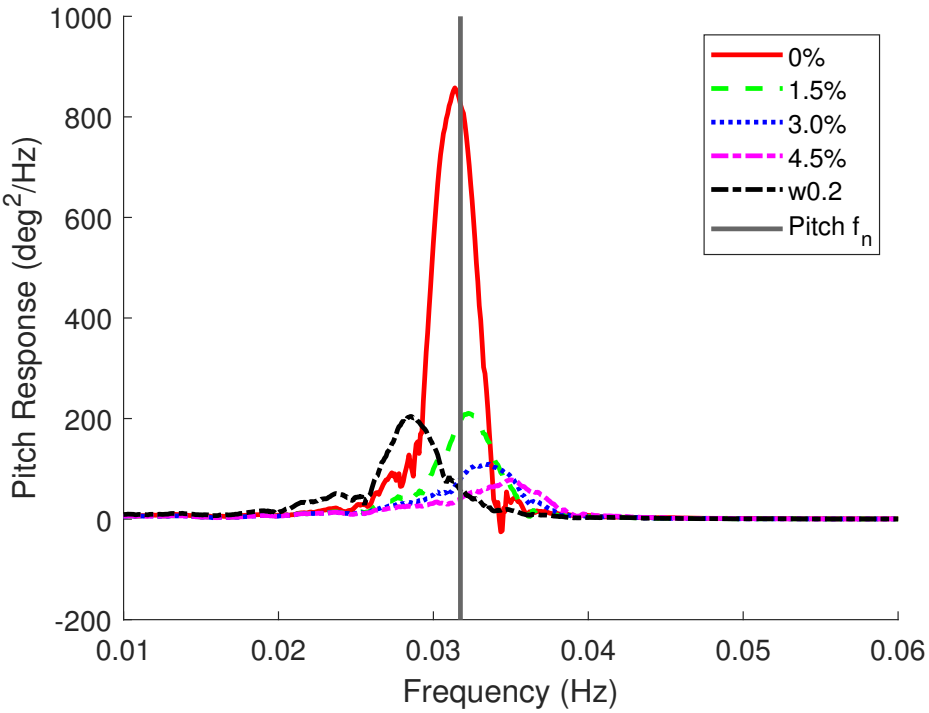

Figure 2.19. Spar platform pitch response, 18 m/s wind case

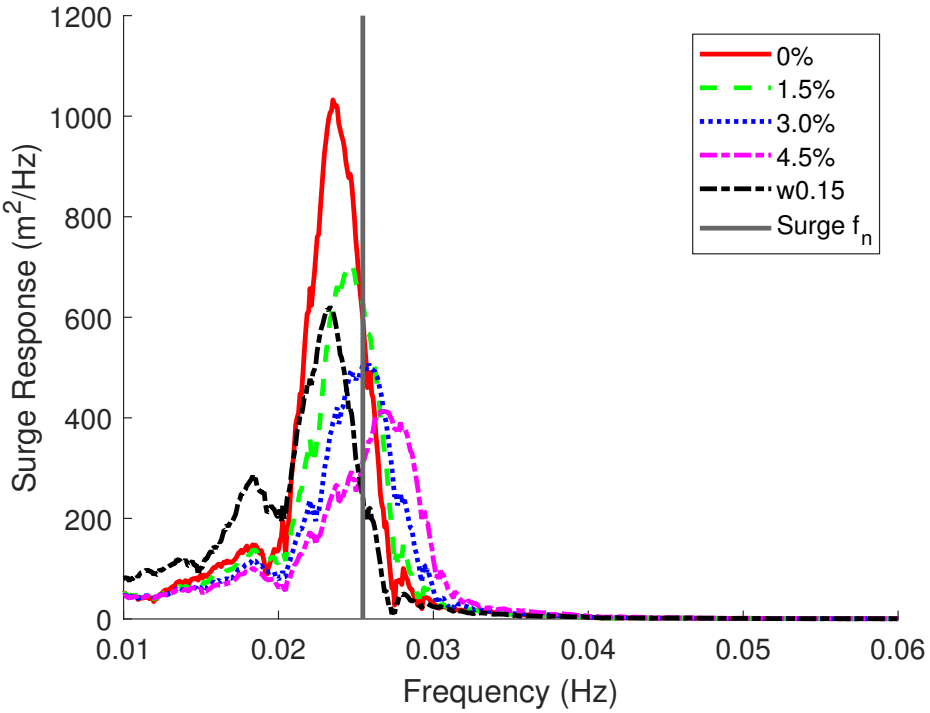

Figure 2.20. TLP platform surge response, 12 m/s wind case

Unlike the semisubmersible and the spar, the DeepCwind TLP's dominant rigid-body mode is in surge. For the 12 m/s mean wind case (Figure 2.20), results follow the same general trend as pitch for the spar. As $\Delta\zeta_{DoF}$ increases, peak response magnitude decreases and peak response frequency increases. However, the low $\omega_{n,rot,des}$ of the detuned controller relative to the other platforms results in higher surge response than the 3.0% or 4.5% controllers.

The trend of poor detuned controller performance continues for the 18 m/s mean wind case, shown in Figure 2.21. It exhibits performance worse than even the 0% controller. One additional point of interest is that the effect of peak response frequency shifting with $\Delta\zeta_{DoF}$ is less pronounced than for the other turbines and load cases.

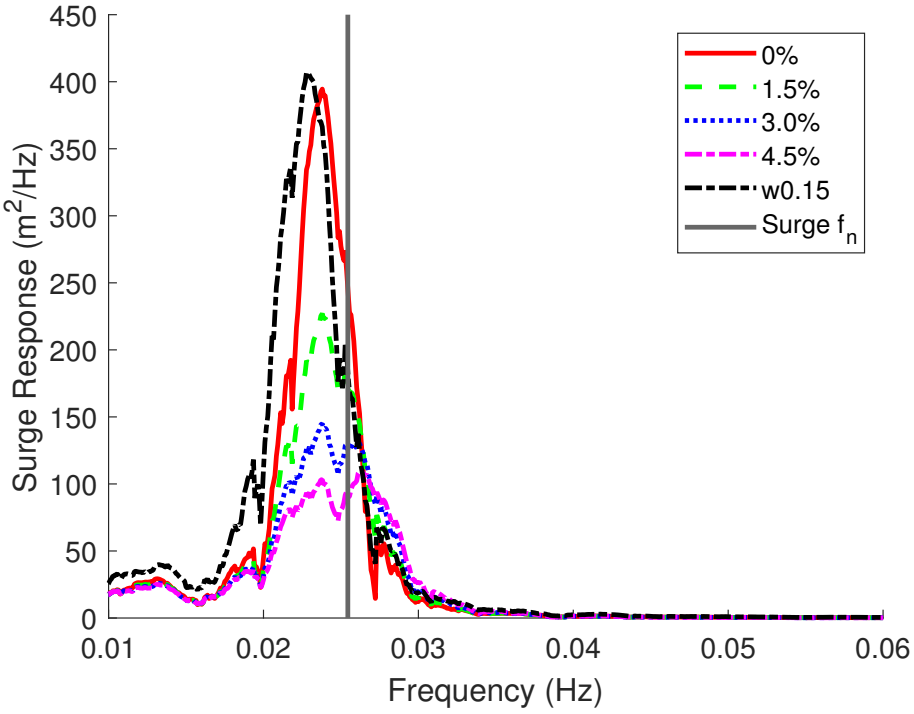

Figure 2.21. TLP platform surge response, 18 m/s wind case

CHAPTER 3
STRUCTURAL CONTROL FEASIBILITY

The feasibility of integrating tunable TMDs into the hull of a FOWT is examined in this chapter. This has been broken down into three components. First, the power consumed by compressors required to adjust the settings of the dampers is quantified. Off-axis system performance is evaluated by looking at load cases where waves approach at -45 degrees relative to the cruciform hull. Finally, the potential for harnessing the power dissipated by the TMDs is evaluated.

3.1 Overview of Ducted Fluid Absorbers

The tunable TMD technology being considered is known as a ducted fluid absorber (DFA), shown in Figure 3.1 and developed in [25]. DFAs utilize ballast water as a damper mass, using air as a spring and a reed valve or similar device to regulate the damping. By adjusting the pressure of the air reservior, the natural frequency of the DFA can be changed.

3.2 Simulation Tools

Two models were used in this study. A frequency domain model developed in [41] was used for finding the best-performing damper configurations. This model considers platform translations, TMD motions, and tower deformations. Wave forcing is calculated using WAMIT [42].

To verify the results from the frequency domain model and perform the off-axis and power consumption studies, a modified version of NREL's OpenFAST time-domain simulation software was used, as described in [25]. In this version of the software, TMDs are modeled as discrete bodies that can move along a single DoF. Forces and moments

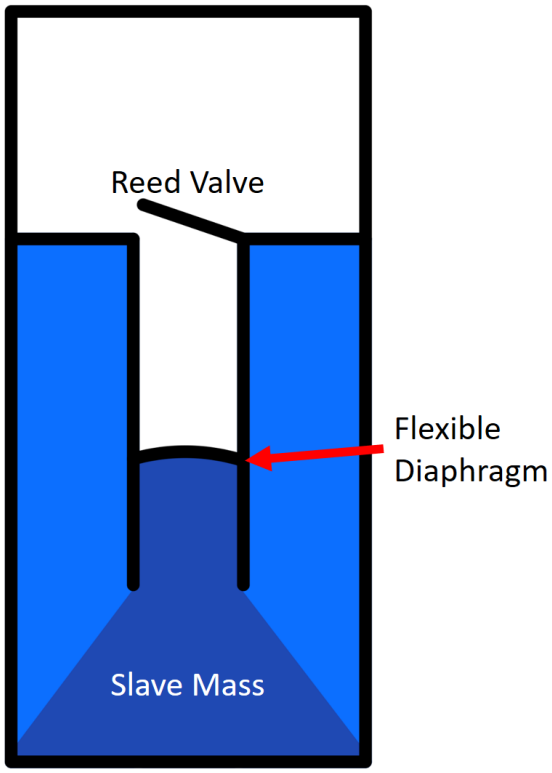

Figure 3.1. A simple diagram of a ducted fluid absorber, reproduced from [25]

associated with the dampers were applied to the rest of the platform through HydroDyn, the hydrodynamics component of OpenFAST.

3.3 Demonstration System

A specialized floating platform was utilized for the study of the tunable TMDs, shown in Figure 3.2 and developed in [41]. General properties of the cruciform hull are given in Table 3.1. The wind turbine design and blade pitch controller for this model come from the

Table 3.1. Demonstration system general properties

Property	Value
Displaced Volume	18826.5m^3
Platform Mass (excl. TMDs)	$1.2808 \times 10^7\text{kg}$
Roll Inertia	$2.874 \times 10^9\text{kgm}^2$
Pitch Inertia	$2.874 \times 10^9\text{kgm}^2$
Yaw Inertia	$5.748 \times 10^9\text{kgm}^2$

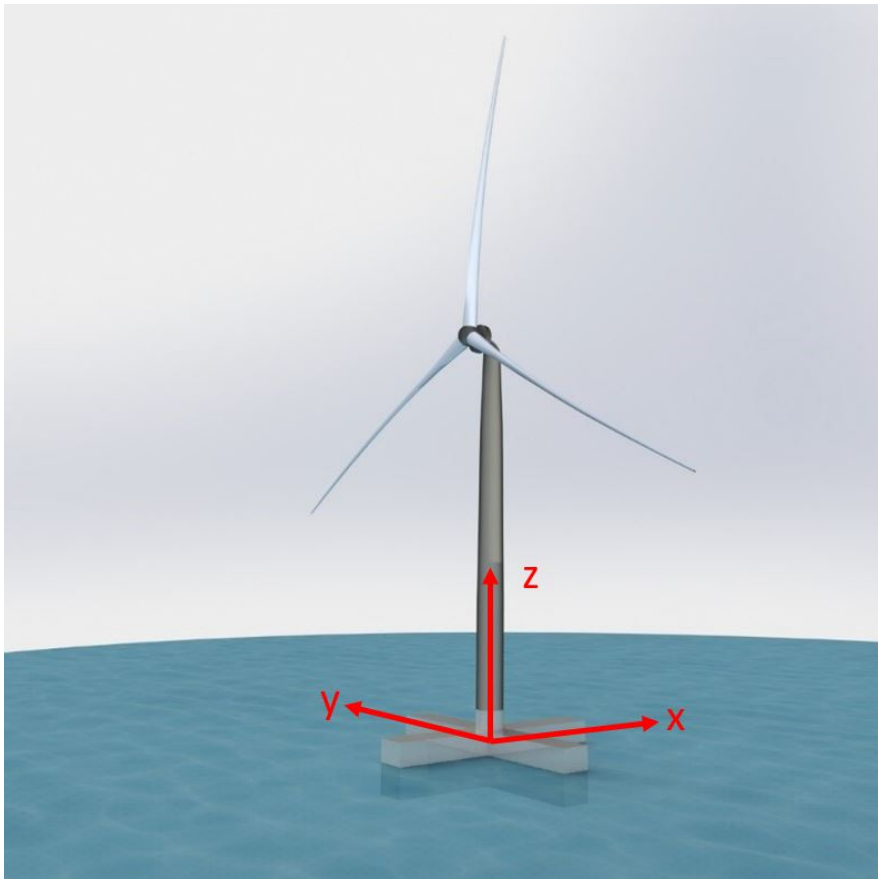

Figure 3.2. The examined cruciform FOWT platform, reproduced from [41]

IEA 15MW reference wind turbine [43]. The center of gravity of the dampers are located at 34.2 meters radially from the center of the hull and 1.3 meters below the still water line.

Based on early analysis, a grid of hull configurations was examined with periods ranging from 7.74 seconds to 11.1 seconds in 0.42 second increments and having damping ratios ranging from 5 to 25 percent in 5 percent increments. Platform heave RAOs were calculated using the aforementioned frequency domain model.

3.4 Compressor Power Consumption

A major factor in considering the feasibility of the DFAs is how much power the air compressors needed to run them require. To determine this, significant wave height and peak period data from a wave buoy dataset was used to build a set of wave power

spectrums with which to evaluate various hull configurations. A cost function is used to identify the best-performing hull configuration, and then several control regime rules are implemented to dictate when the hull configuration is changed. In this study, heave was the platform motion targeted. Expansion work from increasing the damper pressure is calculated as the hull configuration is changed, and by using the average time between pressure changes and the expected life of the turbine, the average power consumption of the compressors can be calculated.

3.4.1 Obtaining Environmental Conditions

A JONSWAP wave power spectrum can be constructed from significant wave height, peak period, and a peak shaping factor, γ. Significant wave heights and peak periods used in this study were recorded hourly by the NERACOOS E01 buoy in the Gulf of Maine between January 2002 and June 2020 [44]. The last required value to build a JONSWAP spectrum is γ. An empirical relationship between H_s and γ from [45], outlined in Table 3.2, was used to find this value.

Table 3.2. JONSWAP γ at various significant wave heights

Significant Wave Height (m)	γ
0 – 1.2	1.5
1.2 – 2.05	1.6
2.05 – 2.65	1.7
2.65 – 3.4	1.8
3.4 – 4.2	1.9
4.2 – 4.9	2
>4.9	2.75

The JONSWAP spectrum was calculated using the methods from [46], as follows. The JONSWAP spectrum is a derivative of the Pierson-Moskowitz spectrum S_{PM}, defined as

$$S_{PM}(\omega) = \frac{5}{16} H_s^2 \omega_p^4 \omega^{-5} exp(-\frac{5}{4}(\frac{\omega}{\omega_p})^{-4}), \tag{3.1}$$

where $\omega_p = 2\pi/T_p$. The JONSWAP spectrum can then be expressed as

$$S_J(\omega) = (1 - 0.287\ln(\gamma)) S_{PM}(\omega) \gamma^{exp(-0.5(\frac{\omega-\omega_p}{\sigma\omega_p})^2)} \tag{3.2}$$

where σ is

$$\sigma = \begin{cases} 0.07 & \omega \leq \omega_p \\ 0.09 & \omega > \omega_p \end{cases} \tag{3.3}$$

This process was repeated for each hourly data point recorded by the wave buoy.

3.4.2 Cost Function

The standard deviation of a given hull motion can be described as

$$\sigma^2 = S(\omega)|H(\omega)|^2 d\omega \tag{3.4}$$

where $S(\omega)$ is the wave JONSWAP power spectrum and $H(\omega)$ is the hull RAO for the DoF of interest. [47]. This was used as the cost function for the evaluation, so hull configurations that resulted in the least platform heave standard deviation would be chosen.

3.4.3 Evaluated Control Regimes

Several control regimes were examined for determining when to change the hull configuration, as summarized in Table 3.3. 'Dampers off' is the case in which there is no TMD motion relative to the platform. 'Continuous optimum tracking' changes the pressure (frequency) and damping hourly to the best-performing configuration per. the cost function described in the previous section. 'Pressure deadband' only changes to the optimal pressure if the current pressure is off by a certain deadband, but damping is changed such that the optimal configuration is used within the subset with the current pressure setting. This is meant to limit the amount of pressure adjustments, and ergo, the power consumed by the compressors. 'Best pressure' locks the pressure to the setting that works best most of the time, but allows the damping to be adjusted. 'Best configuration' locks both the pressure and damping to the configuration that works best on average.

3.4.4 Expansion Work

After calculating the series of configurations used under each of the different control regimes, the amount of expansion work done by the compressors to increase the TMD

Table 3.3. Evaluated damper control regimes

Regime Type	Pressure Adjustment	Damper Adjustment
Dampers Off	-	-
Continuous Optimum Tracking	Continuous	Continuous
Pressure Deadband	On Exceeding Deadband	Continuous
Best Pressure	None	Continuous
Best Configuration	None	None

pressure was calculated using

$$W = \frac{p_2 V_2 - p_1 V_1}{1 - n} \tag{3.5}$$

where n is 1.4 for air. Work due to temperature change is not considered. This work is summed through the life of the turbine using JONSWAP spectrums from the wave buoy data, and multiplied by four to account for the number of dampers in the hull. The total work is then divided by the turbine life to calculate the average power consumption of the compressor.

3.5 Off-Axis Performance

A unique loading condition that was considered is when incoming waves strike at a -45 degree angle. While two dampers have an effective lever arm of L_{damp} from the center of gravity and the other two have no lever arm for zero-degree incoming waves, for the -45-degree wave heading case all four dampers have an effective lever arm of $L_{damp}/\sqrt{2}$. Because rotational inertia depends on the lever arm squared, in theory the different arrangements should perform similarly. To test if this is the case, two sea states were considered; one operational condition (equivalent to that for 18 m/s wind) and one extreme (equivalent to 58.7 m/s wind), with the JONSWAP wave environments built up as described in the previous section. Six random seeds of each environment were simulated in the modified OpenFAST program for 600 seconds with a 1000 second lead-in time. Aerodynamic effects were turned off for these simulations. As a baseline for comparison, results for head-on waves and wind were produced alongside the -45 degree results. Several

damper setups were investigated for these conditions; one with all of the dampers turned off ('Off'), one with all of the dampers targeting the pitch natural frequency of the platform ('Pitch'), and one where the fore and aft (with respect to head-on waves) dampers target pitch while the side dampers target heave ('Split').

3.6 Damper Power Dissipation

In the earlier section detailing power consumption, an assessment of the power used by the compressors to adjust the settings of the dampers was described. Ideally, this power is minimized because it is leached from the power generated by the turbine. In this section, the amount of power from incoming waves dissipated by the dampers is assessed. If enough power is dissipated, it may be worth considering harnessing it to generate additional electricity. Simulation environments and setup were identical to those in the "Off-Axis Performance" section, but with OpenFAST configured to model aerodynamic effects. Power dissipated by each of the four dampers was found using the relationship

$$P_{damp} = cv_{damp}^2. \tag{3.6}$$

Damper velocities are given in a TMD output file from the modified version of OpenFAST. The power from each of the dampers is summed to obtain the total power dissipated at each instant, and then this value is averaged for the length of the simulation and for all six seeds.

3.7 Results

3.7.1 Compressor Power Consumption

The ideal setpoints for TMD stiffness and damping, along with the associated effective damper mass and pressure are shown with respect to sea state in Figure 3.3. It can be seen that higher damper pressures (and therefore lower target periods) work better for smaller wave heights. Damping ratio optimized by the cost function only deviates from 10% in extremely small and large wave environments.

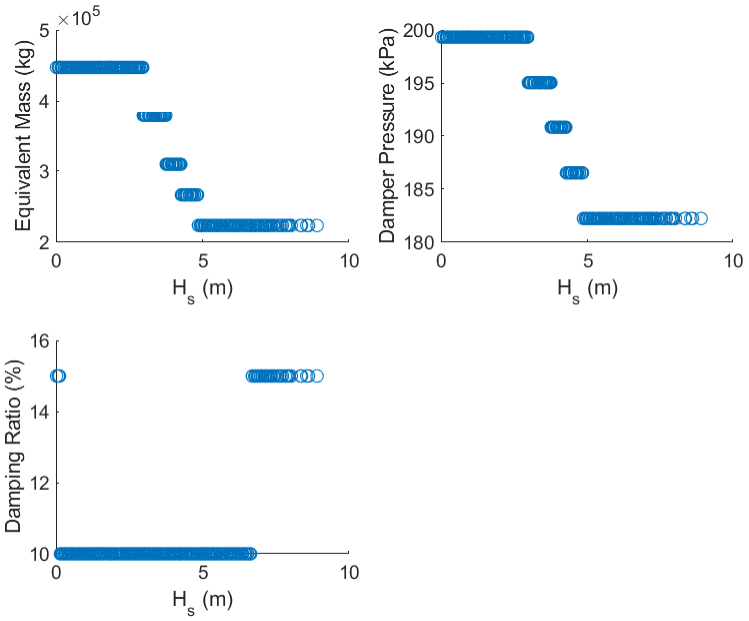

Figure 3.3. Schedule of cost-function minimizing damper settings, plotted vs. significant wave height

Example time domain results for the continuous optimum tracking and 12 kPa deadband regimes are given in Figure 3.4. The 12 kPa deadband is exceeded twice in early March when pressure drops from 199 kPa to 182 kPa and then bounces back to 195 kPa. Afterwards, the optimal pressure is always less than 12 kPa away from the current pressure, so the deadband controller hunts through different damping ratios while the continuous optimal tracking controller can change the pressure. Platform heave standard deviation is extremely similar for both controllers. This means that the deadband controller could produce reductions in fatigue on the structure similar to the continuous optimal tracking controller while consuming less power in adjusting the TMD pressure.

Statistics calculated for the lifetime of the turbine are given in Table 3.4. The mean heave standard deviation (σ) refers to the mean heave standard deviation between all environments over the life of the turbine. Maximum heave standard deviation refers to the single largest heave standard deviation recorded. The annual energy consumption is calculated under the assumption that four dampers are used and the compressor is 20%

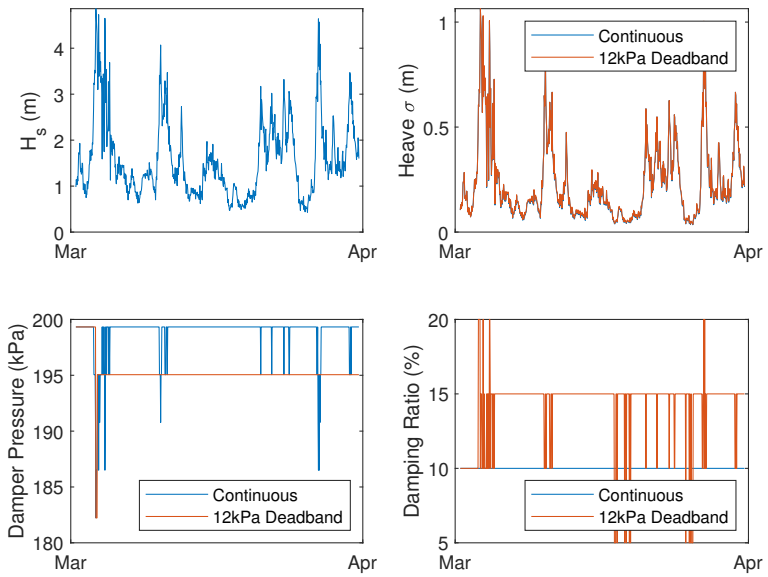

Figure 3.4. Example time domain results for continuous optimal tracking and 12 kPa deadband control regimes

efficient. The gross annual energy production (AEP) of the turbine was obtained from [43] as 77.4 GWh. Using this figure, the percentage of AEP that the compressors consume was calculated.

Between having the dampers off and continuously tracking the optimal setpoint, there is an 18.3% decrease in the mean heave standard deviation and a 2.86% decrease in the maximum heave standard deviation. Going from continuous tracking to a single configuration results in only a 0.12% increase in mean heave standard deviation and a 0.99% increase in maximum heave standard deviation. This suggests that there is a large improvement in heave performance between using dampers and not, but actively tuning the damper provides a smaller return in comparison. The power consumed by the compressors is negligible, with the largest amount being less than a tenth of a percent of the annual energy production. For reference, generator losses converting mechanical power to electrical are around 5.6% [34].

Table 3.4. Tunable damper power consumption statistics

Control Regime	Mean Heave σ (m)	Max Heave σ (m)	Mean Pressure Increases/Day	Annual Energy Consumption (kWh)	Percentage of Gross AEP
Dampers Off	0.1939	2.219			
Continuous Tracking	0.1585	2.155	0.3977	24170	0.031%
8 kPa Deadband	0.1602	2.155	0.530	6172	0.008%
12 kPa Deadband	0.1618	2.155	0.0182	3104	0.004%
16 kPa Deadband	0.1585	2.155	0.0155	3422	0.004%
Single Pressure (199.3 kPa)	0.1586	2.162			
Single Configuration (199.3 kPa, 10% damping)	0.1587	2.176			

3.7.2 Off-Axis Performance

On- (zero degrees) and off-axis (-45 degrees) heave standard deviation results for the 18 m/s wind case are shown in Figure 3.5. For any given TMD setting, the off axis heave standard deviation is lower than for on-axis. Predictably, pitch-targeting dampers resulted in a higher standard deviation than the setting split between heave and pitch.

In the larger sea state with 58.7 m/s mean wind shown in Figure 3.6, the results are much closer but still slightly smaller for the -45 degree waves. Either setting with dampers provides an advantage to having the dampers off, though the split targeted dampers still provides an advantage over the pitch-targeted setting.

Hydrodynamic stiffness and inertia values are identical between the on- and off-axis wave cases, so the primary difference in performance comes down to the heave forcing of the system. Obtained from WAMIT results, Figure 3.7 shows how the zero-degree wave case has higher forcing in smaller wave periods as would occur during the 18 m/s wind case, and the gap tightens as the sea state grows.

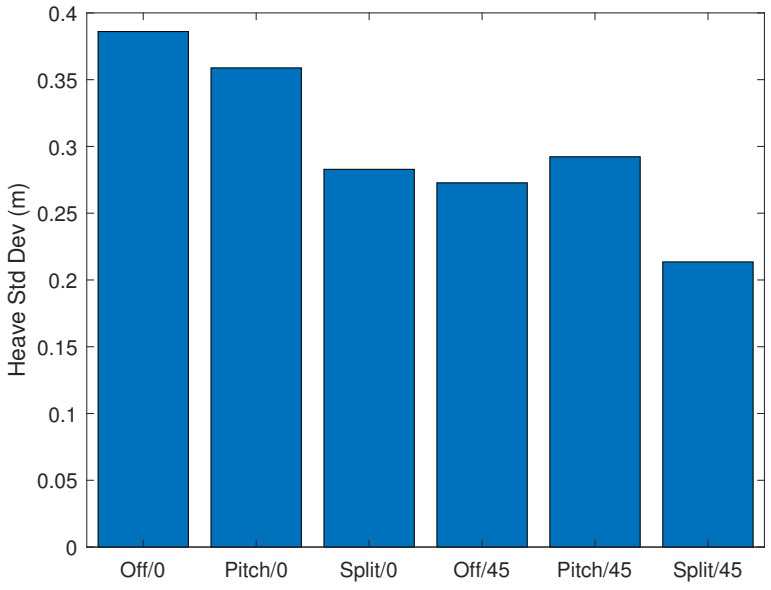

Figure 3.5. Heave standard deviation for various TMD layouts, 18 m/s wind case

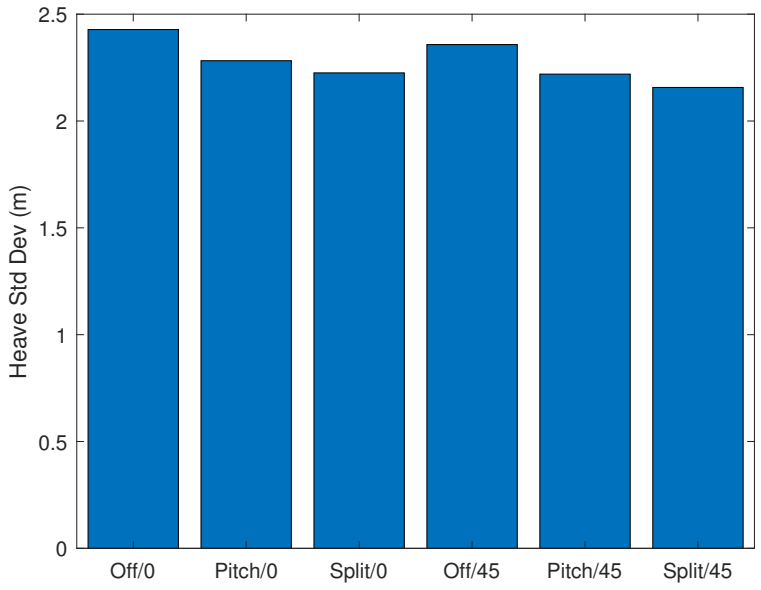

Figure 3.6. Heave standard deviation for various TMD layouts, 58.7 m/s wind case

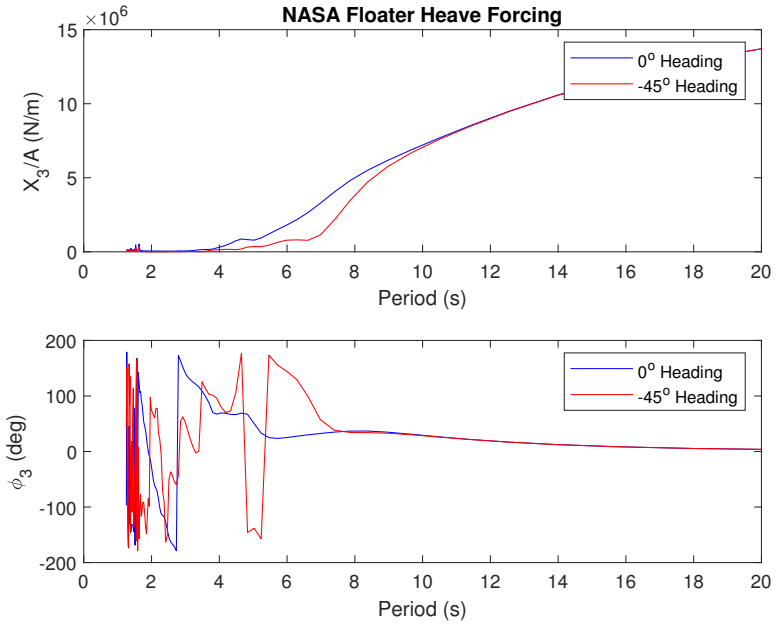

Figure 3.7. Heave forcing on the platform

Trends similar to heave can be noted for heel (combined pitch and roll). For the 18 m/s load case shown in Figure 3.8, heel standard deviation for on-axis waves is roughly twice what it is for -45-degree waves using the same TMD layout. The pitch-targeting and split settings perform roughly equivalently for the on-axis waves, which makes sense given that the fore and aft dampers that have a lever arm are tuned identically.

In the extreme wave environment shown in Figure 3.9, the gap between on- and off-axis heel standard deviation performance narrows similar to how it did with heave. The pitch-targeted dampers work marginally better for both incoming wave directions than the split dampers, though either setting produces roughly a third less heel standard deviation than having the dampers off.

Once again, the differences in performance between wave headings can be explained by heel forcing for the platform, seen in Figure 3.10. The -45-degree heading tends to produce less forcing in small sea states, while performance is more similar for large sea states.

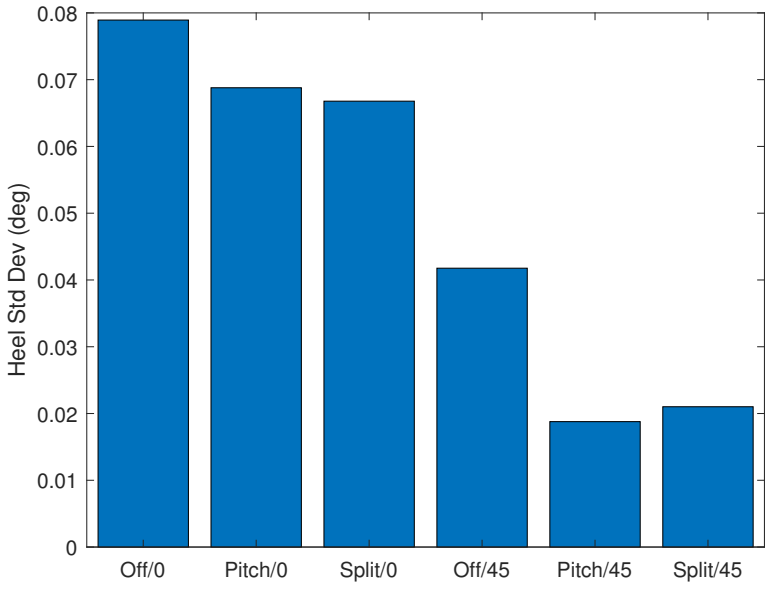

Figure 3.8. Heel standard deviation for various TMD layouts, 18 m/s wind case

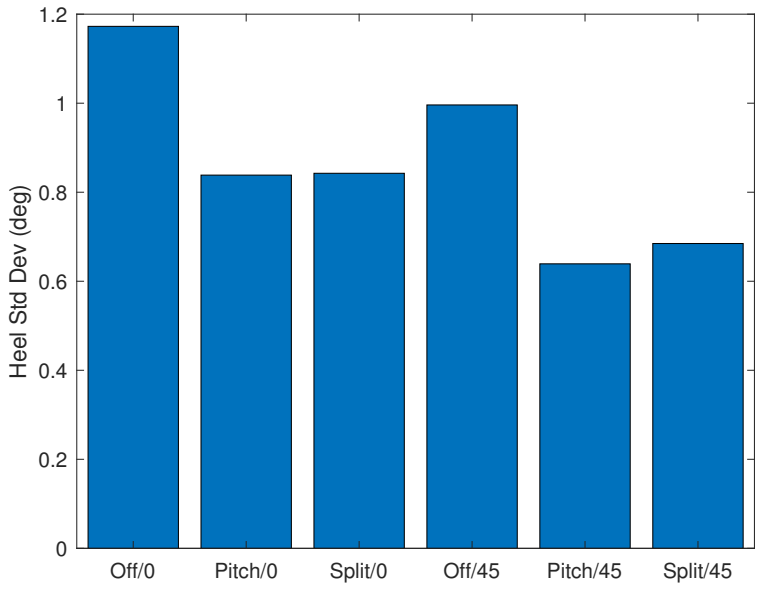

Figure 3.9. Heel standard deviation for various TMD layouts, 58.7 m/s wind case

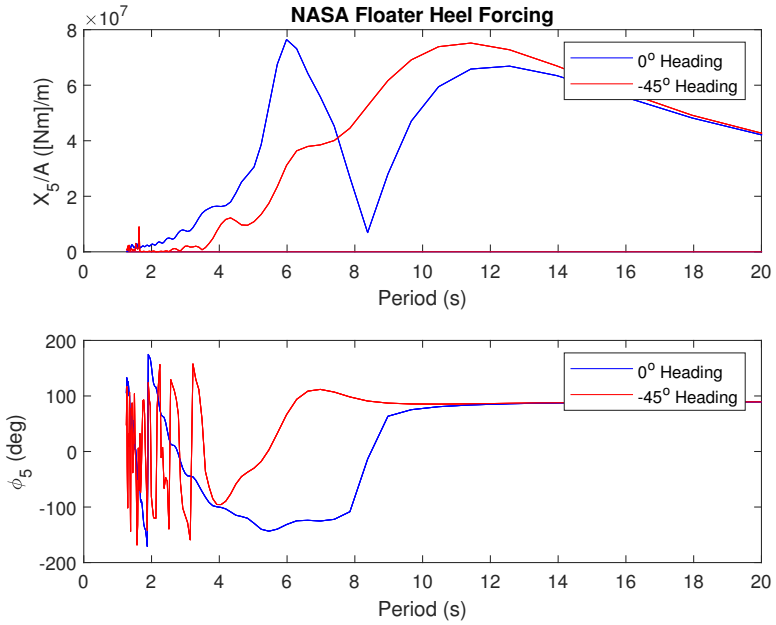

Figure 3.10. Heel (combined pitch and roll) forcing on the platform

3.7.3 Damper Power Dissipation

Average power dissipated by the dampers in operational and extreme environments is shown in Table 3.5. Five megawatts are dissipated in the extreme environment, which is a third of the nameplate capacity of the turbine itself. This makes it tempting to contemplate putting a device into the dampers to generate more electrical power. However, this result is for a fifty-year event; much less power (around one half of one percent of the turbine's nameplate capacity) is dissipated by the dampers in day-to-day operational conditions. Compounding this issue is the matter of electricity-generating devices not being 100% efficient, so only a fraction of the mechanical power dissipated by the TMDs could be captured.

Table 3.5. Power Dissipated by Dampers

DLC 1.2, 18m/s wind (operational)	DLC 6.1, 58.7m/s wind (50 year)
85.0 kw	5098 kw

CHAPTER 4
STRUCTURAL CONTROL IMPLEMENTATION

This chapter describes the development of a map of pitch motion-minimizing TMD settings relative to sea state peak period and a controller for a floating offshore platform with tunable TMDs. After completing the feasibility study described in the last chapter, some of the goals and assumptions in the overarching project were changed. In this chapter, the target motion for reduction is pitch rather than heave. The effective mass is treated as constant rather than varying with TMD setting due to developments with the damper technology. This work is presented in part in [28].

4.1 Controller Overview

The TMD setting controller was developed for the floating system described in [41], and shown in Figure 4.1 For the development of the controller, the effective TMD mass was assumed to be a constant 856,640 kg.

An overview of the workings of the TMD controller is shown in Figure 4.2. The significant wave height and peak period of the wave envirnoment are calculated using a sea state estimator as described in [28]. This estimator uses time-domain wave height data from a wave-rider buoy. From here, the wave environment is compared against a map of TMD settings developed using the frequency domain model described in the previous chapter. The TMD controller decides which setting to use based on this map, and then makes the change to the TMD setting. This change then affects the system, as represented by the modified version of OpenFAST also described in the previous chapter.

4.2 Setting Schedule Using Frequency Domain Model

The optimal damper setting per. Equation 3.4 was found for a set of design load cases (DLCs) described in Table 4.1. A grid of TMD settings ranging from 5% to 30% damping

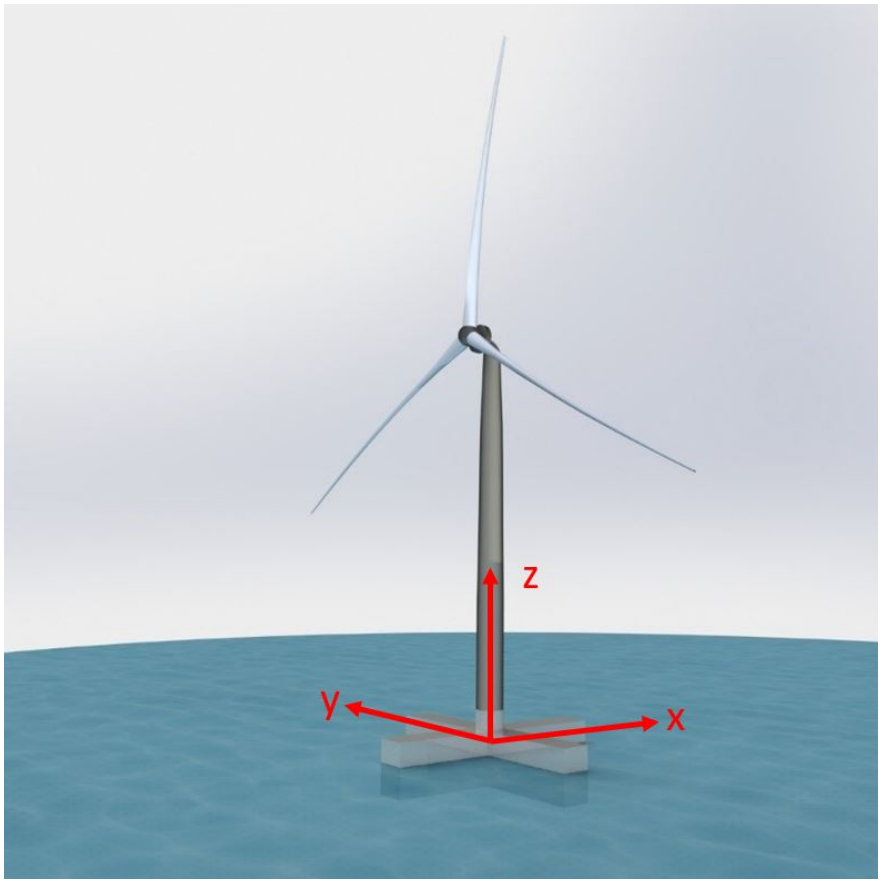

Figure 4.1. The examined cruciform FOWT platform, reproduced from [41]

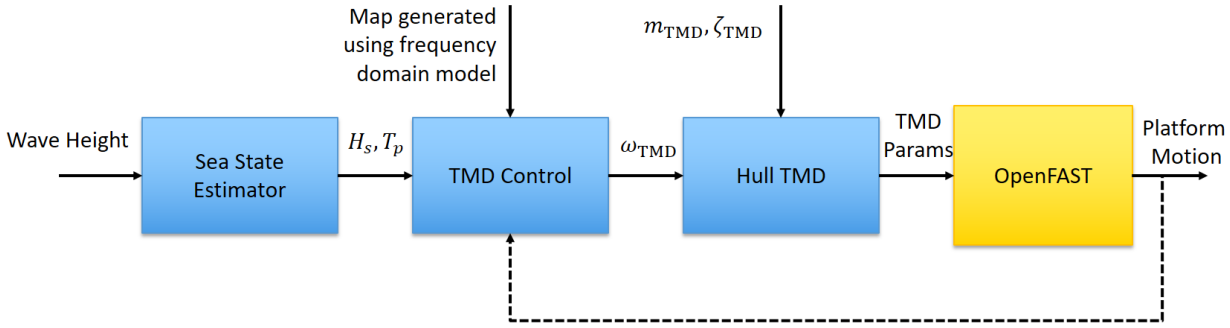

Figure 4.2. TMD controller integration into the OpenFAST simluation framework.

in 5% increments and from 2.5 seconds to 30 seconds target period in 1.25-second increments was searched through for each DLC in order to find the best configuration.

Table 4.1. DLCs studied in this work

DLC	Wind Model	Wave Model
1.2	Normal turbulence, with mean wind speeds from 4–24 m/s in 2-m/s steps, and Class A turbulence	Normal wave model, with T_P from 6.9–9.0 s and H_s from 0.8–3.1 m, depending on the wind speed
1.6	Same as DLC 1.2	Extreme wave model, with T_P from 11.5–14.1 s and H_s from 6.3–9.8 m, depending on the wind speed
6.1	50-year wind speed (58.7 m/s) with Class A extreme turbulence model (ETM) turbulence	50-year wave model (T_P = 14.2 s and H_s = 9.8 m)
6.3	1-year wind speed (44.9 m/s) with Class A ETM turbulence	1-year wave model (T_P = 11.7 s and H_s = 6.4 m)
6.5	500-year wind speed (65.1 m/s) with Class A ETM turbulence	500-year wave model (T_P = 15.0 s and H_s = 11.5 m)

4.3 Results

4.3.1 Determining the Controller Setting Schedule

Pitch response standard deviations calculated by the frequency domain model for DLC 1.2 with an 18-m/s wind are shown in Figure 4.3. While adjusting the damping ratio has a minimal impact on damper performance, there is a clear trough with respect to frequency. The damper natural frequency found to minimize the platform pitch response in this case was 1.2566 rad/s. At this TMD frequency, the damping ratio that minimizes pitch response is 5%. However, platform pitch response only changes by four percent when the damping ratio is increased to 30%.

Similar trends for damping ratio and TMD frequency can be noted for DLC 6.1, as seen in Figure 4.4. The difference this time is that a lower TMD frequency of 0.4570 rad/s minimizes the platform pitch response. The damping ratio for minimal pitch response is again 5%. The response increases by 8.3% if the damping ratio is increased to 30% at this TMD frequency.

Based on the results in Figs. 4.3 and 4.4, the TMD damping ratio was locked to 5% when creating a lookup table of optimal TMD settings. The TMD natural frequencies

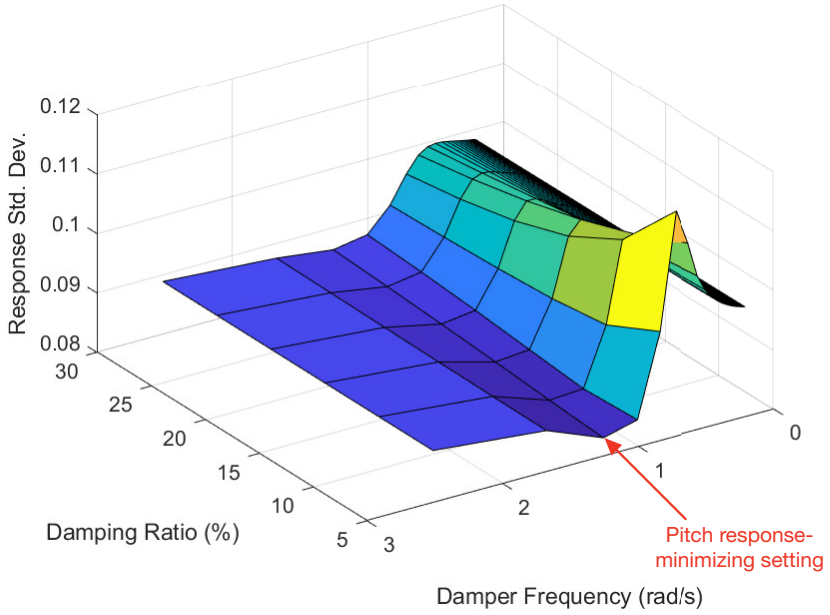

Figure 4.3. Pitch response standard deviation for various TMD settings; DLC 1.2 for an 18-m/s wind

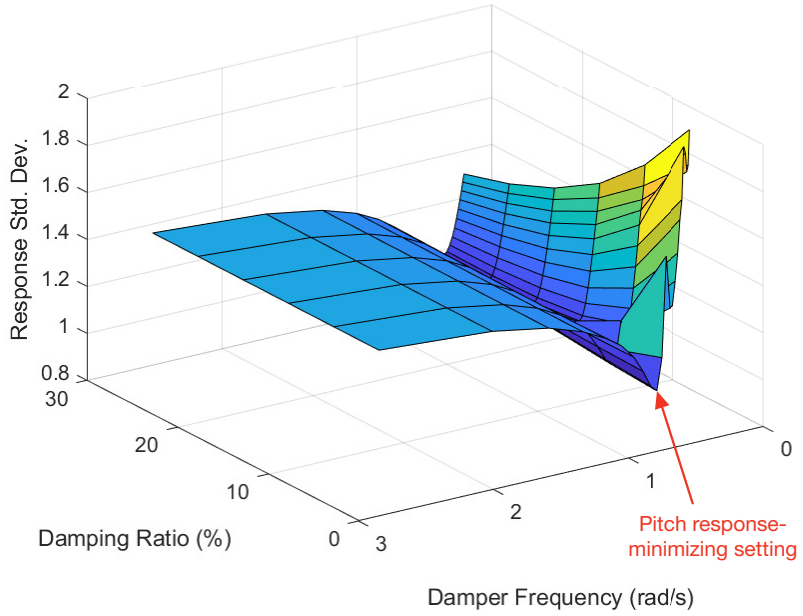

Figure 4.4. Pitch response standard deviation for various TMD settings; DLC 6.1

producing the least pitch response were recorded for the DLCs in Table 4.1, and then a piecewise linear function was fitted to the data. This is shown in Figure 4.5. Of note, there

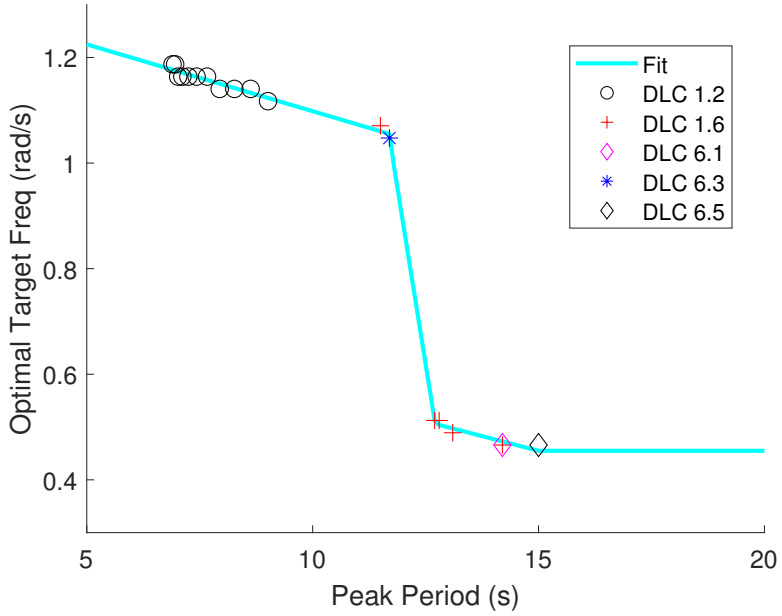

Figure 4.5. Optimal damper frequency for several wave environments and piecewise linear fit

is a large drop off in the best-performing TMD natural frequency between environments with a peak period of 11.7 seconds and 12.7 seconds. This drop off was found to be due to minute differences in the RAOs of the different damper settings. The JONSWAP spectrum for peak periods of 11.7 and 12.7 seconds, along with platform pitch RAOs for TMD natural frequencies of 1.07 rad/s (optimal setting for $T_p = 11.7$ s) and 0.512 rad/s (optimal setting for $T_p = 12.7$ s) and the platform pitch power spectrum densities (PSDs) created by combining the JONSWAP spectrum and RAOs, are shown in Figure 4.6. A small bump in the RAO of the 0.512 rad/s TMD at a frequency of approximately 0.58 rad/s is magnified by being under the peak of the JONSWAP spectrum for an 11.7 second peak wave period, leading to the platform pitch PSD being greater than for the 1.07 rad/s TMD. Because the peak of the JONSWAP spectrum is moved to a lower frequency for a 12.7-second peak wave period, this small bump contributes less to the platform pitch PSD. In effect, the

bump causes the 0.512 rad/s TMD to have a larger pitch standard deviation than the 1.07 rad/s TMD for lower-period wave environments.

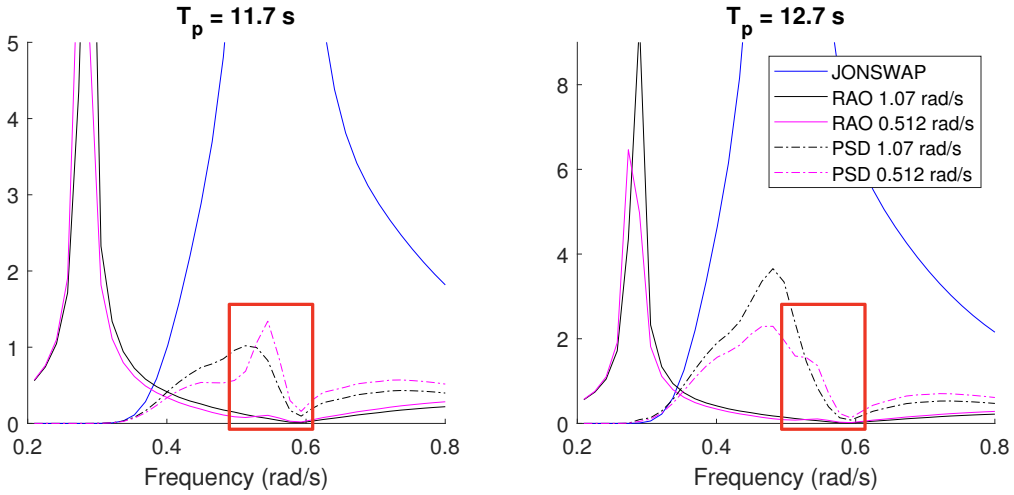

Figure 4.6. Wave power spectrum (m^2/s), RAOs (deg/m), and platform pitch PSDs (deg^2/s) at peak wave periods on either side of the drop in optimal setting

The equation for the piecewise fit function from Figure 4.5 is shown in Table 4.2.

Table 4.2. Piecewise linear fit function for TMD tuning

T_P (s)	Equation
< 11.7	$-0.025T_P + 1.351$
< 12.7	$-0.535T_P + 7.307$
< 15	$-0.022T_P + 0.789$
≥ 15	0.455

4.3.2 Validation with OpenFAST

To verify the frequency domain results, several TMD settings were evaluated in OpenFAST time domain simulations. To examine operational and extreme load cases, six seeds of each setting were examined for DLC 1.2 with an 18-m/s wind and DLC 6.1. Results from the previous section showed that changing the damping ratio has little effect on performance, so all of the examined settings had a damping ratio of 5%. The optimal TMD frequency setting predicted by the frequency domain model was examined, along

with frequencies adjusted from this by ±10%, ±20%, and ±50%. A list of the TMD frequencies tested is provided in Table 4.3.

Table 4.3. TMD natural frequencies examined in OpenFAST

DLC 1.2, 18 m/s (rad/s)	DLC 6.1 (rad/s)
0.6283	0.2285
1.0053	0.3656
1.1310	0.4113
1.2566	0.4570
1.3823	0.5030
1.5079	0.5484
1.8849	0.6855

A comparison of pitch standard deviation performance of different TMD frequencies is shown in Figure 4.7 for DLC 1.2 with an 18 m/s wind. Performance from time domain simulations in OpenFAST are plotted, along with results from the frequency domain model. The optimal TMD frequency predicted by the frequency domain model is shown as a black line. It can be seen that the shape of the data matches very well between the time domain and frequency domain simulations, though there is an offset in predicted pitch standard deviation (the frequency domain model predicts a pitch standard deviation value 22% higher than the time domain simulations at its predicted best-performing frequency).

The gap between the frequency domain predicted results and the time domain simulations tightens for DLC 6.1, as seen in Figure 4.8. Both the frequency domain model and the OpenFAST simulations predict the same TMD frequency to minimize platform pitch standard deviation, and trends in the data are similar for each model.

The similarity in shapes and pitch standard deviation-minimizing natural frequency between the two models means that the predictions of the frequency domain model can be trusted to produce the map of optimal TMD settings. While it would be possible to accomplish this in OpenFAST with results slightly closer to reality, there is a high computational cost to performing time-domain simulations that would be prohibitive in searching the design space for the optimal TMD setting for many environments.

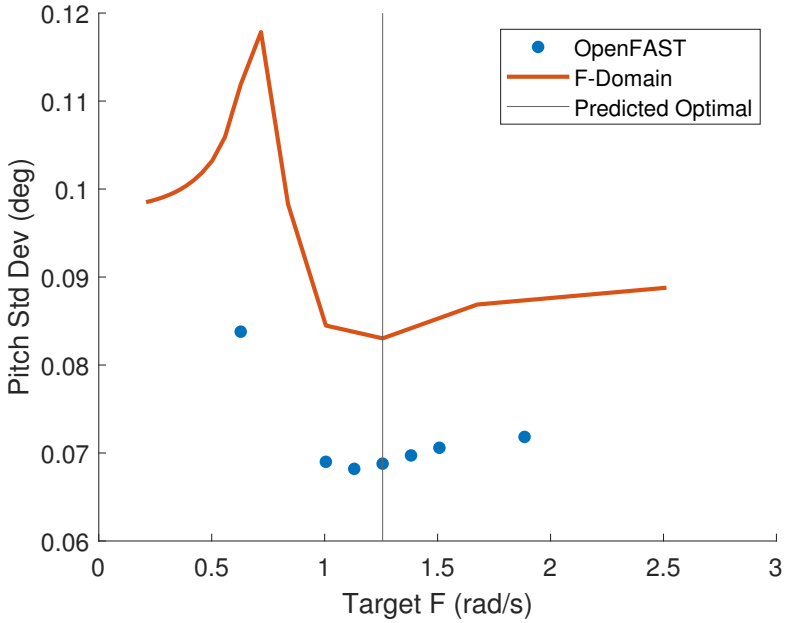

Figure 4.7. OpenFAST time domain pitch standard deviation vs. frequency model predicted values; DLC 1.2 for an 18-m/s wind

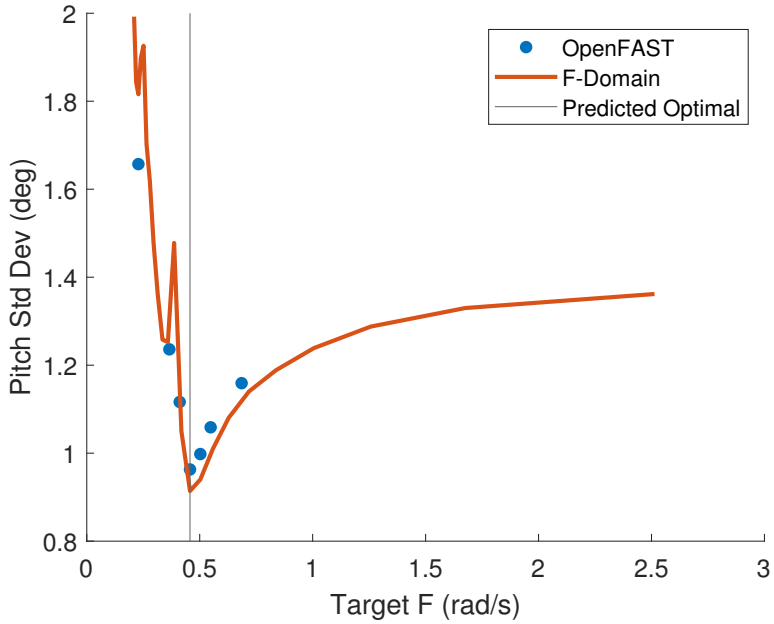

Figure 4.8. OpenFAST time domain pitch standard deviation vs. frequency model predicted values; DLC 6.1

4.3.3 Expanded OpenFAST TMD Schedule Evaluation

The setting schedule for TMD frequencies described here was evaluated in OpenFAST in [28]. Results from this study are reproduced in Figure 4.9. The setting schedules examined include no TMD motion relative to the platform, a TMD locked to the optimal setting for DLC 6.5 ("Const. TMD"), and the gain schedule described in this chapter ("Ideal TMD"). Note that this study assumes perfect knowledge of the wave environment; no sea state estimation is used. From these results, it can be seen that utilizing the TMDs provides significant reductions in fore-aft acceleration, side-to-side acceleration, and pitch standard deviation, among others. However, these same plots also show that tuning the

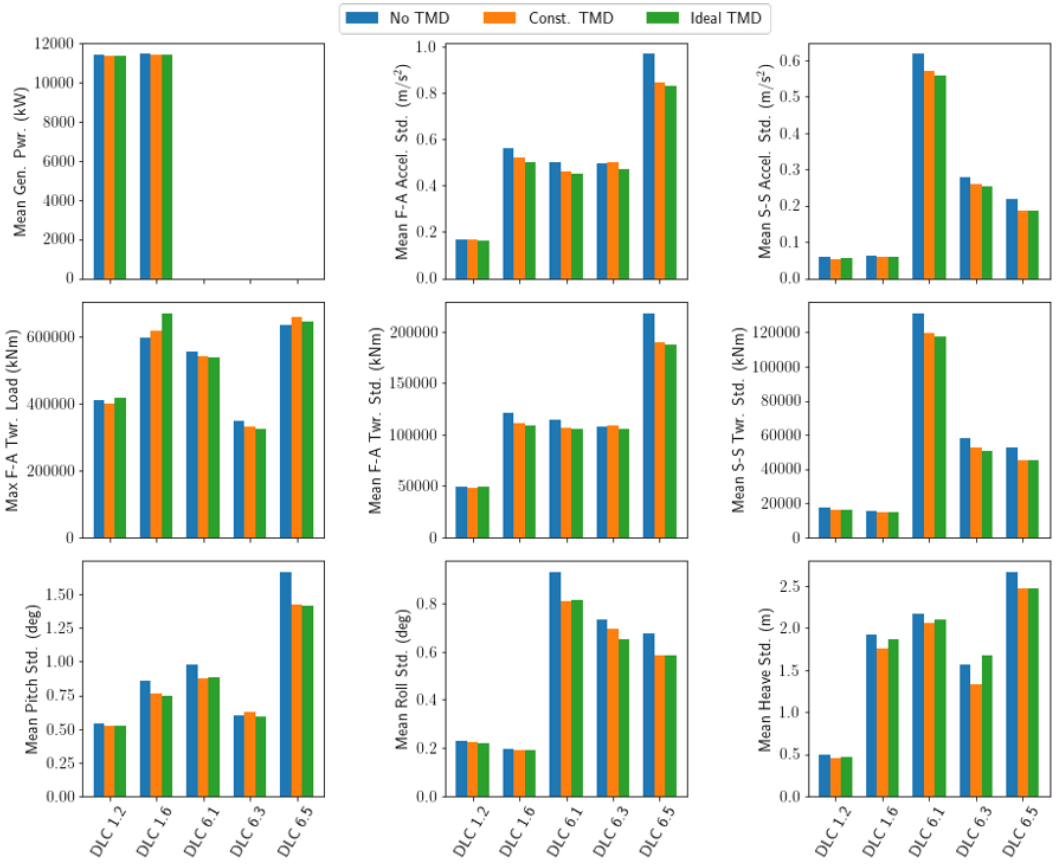

Figure 4.9. Evaluation of several TMD setting schedules in OpenFAST, reproduced from [28]

TMD natural frequency to the wave environment provides only a small improvement relative to the constant TMD setting. A constant TMD setting reduces pitch motion relative to the no-TMD case by 12.0%, while tracking the ideal TMD setting produced a 13.4% reduction. For a few environments and motions, such as DLC 1.6 and 6.3 in heave, the constant TMD setting outperforms following the gain schedule.

CHAPTER 5
CONCLUSIONS

This work considers new developments in blade pitch control and structural control for floating offshore wind turbines in order to improve the management of platform motions and reduce fatigue loads on the structure. For blade pith control, this involved the creation of a new method of scheduling gains utilizing a novel two-DoF model. Regarding structural control, a new type of tunable TMD is examined for potential application to structural control of floating wind turbines.

5.1 Blade Pitch Control With a Two-DoF Model

Many of the following conclusions have been noted in [27], but are reiterated and expanded upon here. A method of obtaining gain schedules for a blade pitch controller was developed for PI controllers with an additional proportional nacelle velocity feedback term using a two-DoF model. This model considers rotor angular displacement and the dominant platform rigid-body mode. Intended to be easily adaptable to various floating wind turbine systems, controllers developed using this method were evaluated in OpenFAST time domain simulations for example semisubmersible, spar, and TLP floaters. The two-DoF controllers were found to provide a middle ground between conventional land-based and detuned controllers, but occasionally outperform both. This was the case in regulating platform pitch and surge range for the spar and TLP, respectively, for an 18-m/s mean wind load condition. Several target increases in platform damping were also compared. Lower increases (1.5%) tended to produce more average power with less variation from this mean. Meanwhile, larger increases in damping (3.0% and 4.5%) tended to produce less response to the dominant rigid-body mode. It was also found that larger increases in target platform damping led to higher platform natural frequencies for the dominant rigid-body mode. Results were mostly consistent between the platforms, indicating that this tuning

method is appropriate for a variety of use cases. Future work in this area will include testing on a larger wind turbine and automation of the gain scheduling process.

5.2 Structural Control Feasibility

Several studies were conducted to assess the feasibility of integrating a new type of tunable TMDs, known as ducted fluid absorbers, into the hull. Adjusting the pressure of air reserviors in the dampers changes their natural frequency and stiffness, while damping could be adjusted with an orifice. The amount of power required to run the compressors to adjust the properties of the ducted fluid absorbers was examined, along with performance in off-axis waves and the potential to harness the power dissipated by the dampers.

5.2.1 Compressor Power Consumption

To evaluate the amount of power consumed by the compressors, possible settings for the dampers were evaluated based on the expected surge standard deviation. This surge standard deviation was calculated from a frequency domain model. Several control schemes were examined, including hourly adjustment to the optimal setting, deadbands to be exceeded before changing damper pressure, the best pressure, and the best single configuration. It was found that power consumption of the compressors was negligible relative to the expected annual power output of the turbine, even for hourly adjustment. Going from no dampers to hourly adjustment resulted in an 18.3% decrease in mean heave standard deviation, though locking the dampers to a single damper configuration resulted in only a 0.12% increase in mean heave standard deviation relative to the hourly adjustment.

5.2.2 Off-Axis Performance

A key load case where waves come at the turbine from a -45-degree angle was examined. Different settings of the TMDs were considered, including all targeting platform pitch, a split setting where the fore and aft (relative to zero degree incoming waves) TMDs

target pitch while the side TMDs target heave, and all dampers off. Operational and extreme sea states were both tested. Heave and heel standard deviation were consistently smaller for the -45-degree wave heading, which can be attributed to differences in heave and pitch forcing on the platform. The all-pitch and split settings performed nearly identically for pitch for a zero degree wave heading, though heave performance was improved with the split setting.

5.2.3 Damper Power Dissipation

Power dissipated by the dampers was also calculated to evaluate the feasibility of harnessing this power to produce more electricity. Though over 5 MW of power is dissipated during a 50-year storm, only 85 kW is dissipated in the operational condition examined. It would not be worth the added complexity to attempt to convert this amount of power into electricity, especially when factoring in the losses associated with the conversion.

5.3 Control of Tunable Hull-Mounted TMDs

A controller was developed for the tunable TMDs by combining a map of settings that minimize platform pitch standard deviation at different sea states with a sea state estimator. It was found that the damping ratio of the TMDs has a smaller effect on the platform pitch standard deviation than their natural frequency, so a piecewise linear function of damper frequency vs. sea state peak period was used as the map of best-performing settings. Several controller frequencies were tested in an operational and extreme sea state in OpenFAST, and it was found that trends in the frequency domain predictions closely mirror the time domain results. Future work in this area would include integration into wind turbine controller tools like NREL's ROSCO.

REFERENCES

[1] Billy Roberts, "Wind resource of the United States: Annual average wind speed at 100 meters above surface level." `https://www.nrel.gov/gis/assets/images/wtk-100m-2017-01.jpg`, 2017. Accessed: 2021-2-19.

[2] W. Musial, D. Heimiller, P. Beiter, G. Scott, and C. Draxl, "2016 offshore wind energy resource assessment for the united states," Tech. Rep. NREL/CP-5000-66599, National Renewable Energy Laboratory, Golden, CO, 2016.

[3] J. Jonkman, "Influence of control on the pitch damping of a floating wind turbine," Tech. Rep. NREL/CP-500-42589, National Renewable Energy Laboratory, Golden, CO, 2008.

[4] T. Larsen and T. Hanson, "A method to avoid negative damped low frequent tower vibrations for a floating, pitch controlled wind turbine," *Journal of Physics, Conference Series*, vol. 75, 2007.

[5] A. Scholbrock, P. Fleming, D. Schlipf, A. Wright, K. Johnson, and N. Wang, "Lidar-enhanced wind turbine control: Past, present, and future," in *Proceedings, 2016 American Control Conference*, (Boston, MA), American Automatic Control Council, 2016.

[6] D. Schlipf, F. Sandner, S. Raach, D. Matha, and P. Cheng, "Nonlinear model predictive control of floating wind turbines," in *Proceedings of the Twenty-Third International Offshore and Polar Engineering Conference*, (Anchorage, AK), International Society of Offshore and Polar Engineers, 2013.

[7] D. Schlipf, E. Simley, F. Lemmer, L. Pao, and P. Cheng, "Collective pitch feedforward control of floating wind turbines using lidar," in *Proceedings of the Twenty-Fifth International Offshore and Polar Engineering Conference*, (Kona, Big Island, HI), International Society of Offshore and Polar Engineers, 2015.

[8] S. Navalkar, J. van Wingerden, P. Fleming, and G. van Kuik, "Integrating robust lidar-based feedforward with feedback control to enhance speed regulation floating wind turbines," in *Proceedings, 2015 American Control Conference*, (Chicago, IL), American Automatic Control Council, 2015.

[9] K. Magar and M. Balas, "Adaptive individual blade pitch control to reduce platform pitch motion of a floating offshore wind turbine: Preliminary study," in *Proceedings of the 2014 ASME Conference on Smart Materials, Adaptive Structures, and Intelligent Systems*, (Newport, RI), American Society of Mechanical Engineers, 2014.

[10] F. Lemmer, D. Schlipf, and P. W. Cheng, "Control design methods for floating wind turbines for optimal disturbance rejection," *Journal of Physics, Conference Series*, vol. 753, 2016.

[11] V. Pascu, S. Kanev, and J. van Wingerden, "Adaptive tower damping control for offshore wind turbines," *Wind Energy*, vol. 20, pp. 765–781, 2017.

[12] K. Kakita, H. Naoyuki, and K. Konishi, "Pi controller gain tuning with frit in collective blade pitch control of floating offshore wind turbines," in *Proceedings, 15th International Conference on Control, Automation, and Systems*, (Busan, South Korea), Institute of Control, Robotics, and Systems, 2015.

[13] B. Fischer, "Reducing rotor speed variations of floating wind turbines by compensation of non-minimum phase zeros," *IET Renewable Power Generation*, vol. 7, no. 4, pp. 413–419, 2013.

[14] B. Fischer and P. Loepelmann, "Balancing rotor speed regulation and drive train loads of floating wind turbines," *Journal of Physics, Conference Series*, vol. 753, 2016.

[15] P. Fleming, A. Peiffer, and D. Schlipf, "Wind turbine controller to mitigate structural loads on a floating wind turbine platform," in *Proceedings of the ASME 35th International Conference on Ocean, Offshore, and Arctic Engineering*, (Busan, South Korea), American Society of Mechanical Engineers, 2016.

[16] M. Lackner, "An investigation of variable power collective blade pitch control for load mitigation of floating wind turbines," *Wind Energy*, vol. 16, pp. 519–528, 2013.

[17] B. Skaare, T. Hanson, and F. Nielsen, "Importance of control strategies on fatigue life of floating wind turbines," in *Proceedings of the 26th International Conference on Offshore Mechanics and Arctic Engineerings*, (San Diego, CA), International Society of Offshore and Polar Engineers, 2007.

[18] N. Abbas, A. Wright, and L. Pao, "An update to the nrel baseline wind turbine controller," Tech. Rep. NREL/CP-5000-75433, National Renewable Energy Laboratory, Golden, CO, 2020.

[19] G. Housner *et al.*, "Structural control: Past, present, and future," *Journal of Engineering Mechanics*, vol. 123, no. 9, pp. 897–971, 1997.

[20] M. Lackner and M. Rotea, "Passive structural control of offshore wind turbines," *Wind Energy*, vol. 14, pp. 373–388, 2010.

[21] Y. Si, H. R. Karimi, and H. Gao, "Modelling and optimiztion of a passive structural control design for a spar-type floating wind platform," *Engineering Structures*, vol. 69, pp. 168–182, 2014.

[22] S. Park, M. Lackner, P. Pourazarm, A. R. Tsouroukdissian, and J. Cross-Whiter, "An investigation on the impacts of passive and semiactive structural control on a fixed-bottom and a floating offshore wind turbine," *Wind Energy*, vol. 22, pp. 1451–1471, 2019.

[23] X. Li and H. Gao, "Load mitigation for a floating wind turbine via generalized H_∞ control," *IEEE Transactions on Industrial Electronics*, vol. 63, no. 1, pp. 332–342, 2016.

[24] Y. Hu and E. He, "Active structural control of a floating wind turbine with a stroke-limited hybrid mass damper," *Journal of Sound and Vibration*, vol. 410, pp. 447–472, 2017.

[25] C. Allen, A. Goupee, J. Lindner, and R. Berry, "Simulation of a floating offshore wind turbine with an integrated response mitigation technology," in *Proceedings of the 1st International Offshore Wind Technology Conference*, (San Fransisco, CA), American Society of Mechanical Engineers, 2018.

[26] E. Lenfest, A. Goupee, A. Wright, and N. Abbas, "Tuning of nacelle feedback gains for floating wind turbine controllers using a two-dof model," in *Proceedings of the ASME 39th International Offshore Conference on Ocean, Offshore, and Arctic Engineering*, (Fort Lauderdale, FL), American Society of Mechanical Engineers, 2020.

[27] E. Lenfest, A. Goupee, A. Wright, and N. Abbas, "Two-dof model-informed controller gain tuning for several floating wind platforms," in *Proceedings of the 31st International Offshore and Polar Engineering Conference*, (Rhodes, Greece), International Society of Offshore and Polar Engineers, In Review.

[28] D. Zalkind, M. Shields, E. Lenfest, A. Goupee, and C. Allen, "Open-loop control of adjustable tuned mass dampers for floating wind turbine platforms," in *Proceedings of the 31st International Offshore and Polar Engineering Conference*, (Rhodes, Greece), International Society of Offshore and Polar Engineers, In Review.

[29] A. Robertson *et al.*, "Definition of the semisubmersible floating system for phase ii of oc4," Tech. Rep. NREL/TP-5000-60601, National Renewable Energy Laboratory, Golden, CO, 2014.

[30] J. Jonkman, "Dynamics modeling and loads analysis of an offshore floating wind platform," Tech. Rep. NREL/TP-500-41958, National Renewable Energy Laboratory, Golden, CO, 2007.

[31] S. Rao, *Mechanical Vibrations, Fifth Edition*. Upper Saddle River, NJ: Pearson, 2011.

[32] N. Nise, *Control Systems Engineering, Sixth Edition*. Jefferson City, MO: John Wiley & Sons, 2011.

[33] K. Aström and R. Murray, *Feedback Systems*. Princeton, NJ: Princeton University Press, 2010.

[34] J. Jonkman *et al.*, "Definition of a 5-mw reference wind turbine for offshore system development," Tech. Rep. NREL/TP-500-38060, National Renewable Energy Laboratory, Golden, CO, 2009.

[35] H. Zumbahlen, "Phase response in active filters," *Analog Dialogue*, vol. 50, no. 1, pp. 26–29, 2016.

[36] J. Jonkman, "Definition of the floating system for phase iv of oc3," Tech. Rep. NREL/TP-500-47535, National Renewable Energy Laboratory, Golden, CO, 2010.

[37] A. Goupee, B. Koo, R. Kimball, K. Lambrakos, and H. Dagher, "Experimental comparison of three floating wind turbine concepts," *Journal of Offshore Mechanics and Arctic Engineering*, vol. 136, 2014.

[38] B. Koo, A. Goupee, R. Kimball, and K. Lambrakos, "Model tests for a floating wind turbine on three different floaters," *Journal of Offshore Mechanics and Arctic Engineering*, vol. 136, no. 2, 2016.

[39] "Guidance notes on global performance analysis for floating offshore wind turbines," tech. rep., American Bureau of Shipping, Spring, TX, 2020.

[40] P. Fleming, I. Rossetti, A. Wright, and D. Arora, "Evaluating methods for control of an offshore floating turbine," in *Proceedings of the 33rd ASME International Conference on Ocean, Offshore, and Arctic Engineerings*, (San Fransisco, CA), American Society of Mechanical Engineers, 2014.

[41] C. Allen, A. Goupee, and A. Viselli, "A computationally-efficient frequency domain model of a floating wind turbine with hull-based tuned mass damper elements," in *Proceedings of the 31st International Offshore and Polar Engineering Conference*, (Rhodes, Greece), International Society of Offshore and Polar Engineers, In Review.

[42] "WAMIT user manual, versions 6.4, 6.4pc, 6.3s, 6.3s-pc," tech. rep., WAMIT, Inc., Chestnut Hill, MA, 2006.

[43] E. Gaertner *et al.*, "Definition of the iea wind 15-megawatt offshore reference wind turbine," Tech. Rep. NREL/TP-5000-75698, National Renewable Energy Laboratory, Golden, CO, 2020.

[44] N. Pettigrew, "Neracoos e01 station data." `http://neracoos.org/datatools/realtime/location/?platform=E01`, 2002-2020. Accessed: 2020-6-22.

[45] A. Viselli, *Model Test of a 1:8 Scale Floating Wind Turbine Offshore in the Gulf of Maine*. PhD thesis, University of Maine, Orono, ME, August 2014.

[46] "Environmental conditions and environmental loads," Tech. Rep. DNVGL-RP-C205, DNV GL, Bærum, Norway, 2017.

[47] O. Faltinsen, *Sea Loads on Ships and Offshore Structures*. Cambridge, UK: Cambridge University Press, 1990.

BIOGRAPHY OF THE AUTHOR

Eben J. Lenfest was born in Waterville, Maine and graduated from Skowhegan Area High School as valedictorian in 2015. Raised in the Belgrade Lakes region of Maine, he acquired a passion for spending time in and preserving nature. Eben received his Eagle Scout rank in the Boy Scouts of America in 2015, and spent several summers helping a local conservation group mitigate an invasive aquatic plant infestation.

Eben attended the University of Maine, pursuing a Bachelor of Science degree in Mechanical Engineering. He started working as an undergraduate research assistant at the Advanced Structures and Composites Center in 2018, and spent a summer interning at NASA Marshall Space Flight Center working on applying a novel structural control technology to floating offshore wind turbines. Eben graduated in 2019 as the Outstanding Graduate of the College of Engineering.

Eben began his graduate studies on the topic of controls for offshore wind turbines in 2019. To this end, he spent a summer at the National Renewable Energy Laboratory as a visiting student scholar. Eben has been the recipient of an AVANGRID and an Alfond graduate fellowship. In his free time, Eben enjoys exploring the mountains and lakes of Maine and playing the french horn. He is a candidate for the Master of Science degree in Mechanical Engineering from the University of Maine in May 2021.